DISSIPATION AND EDDY MIXING ASSOCIATED WITH FLOW PAST AN UNDERWATER TURBINE

by

Zaqie Reza

A Thesis Submitted to the Faculty of

The College of Engineering and Computer Science

in Partial Fulfillment of the Requirements for the Degree of

Master of Science

Florida Atlantic University

Boca Raton, Florida

August 2010

DISSIPATION AND EDDY MIXING ASSOCIATED WITH FLOW PAST AN UNDERWATER TURBINE

by

Zaqie Reza

This thesis was prepared under the direction of the candidate's thesis advisor, Dr. Manhar Dhanak, Department of Ocean and Mechanical Engineering, and has been approved by the members of his supervisory committee. It was submitted to the faculty of the College of Engineering and Computer Science and accepted in partial fulfillment of the requirements for the degree of Master of Science.

SUPERVISORY COMMITTEE:

Manhar Dhanak, Ph.D.
Thesis Advisor

Palaniswamy Ananthakrishnan, Ph.D.

Chaouki Ghenai, Ph.D.

Howard P. Hanson, Ph.D.

Mohammad Ilyas, Ph.D.
Chair, Department of Ocean and Mechanical Engineering

Karl K. Stevens, Ph.D., P.E.
Dean, College of Engineering and Computer Science

Barry T. Rosson, Ph.D.
Dean, Graduate College

July 20, 2010
Date

ACKNOWLEDGEMENTS

I would like to thank my advisor, Dr Manhar Dhanak, who has been a source of motivation throughout my tenure here at FAU. I have derived a lot of inspiration from his calm and serene demeanor even in toughest of situations. Without his guidance and help this thesis would not have been possible.

I would like to express my deepest gratitude to my advisory panel members, Dr. Palaniswamy Ananthakrishnan and Dr. Howard P. Hanson, whose timely advice, inputs and encouragement helped me a lot in completion of this thesis. Dr. Chaouki Ghenai, meticulously introduced me to the nuances of CFD packages. Thanks a lot for your patience and time.

Thanks to Center for Ocean Energy Technology, FAU for funding my thesis. Special mention of thanks to Gabriel Alsenas, who provided me with much needed computational resources from whatever he could dispense.

My gratitude to Ranjith, for the timely discussions we had which made me think and apply a lot more, than what I would have. Thanks to Lakitosh, Aneesh and Baishali for being like a family and supporting me.

I wish to express my sincere gratitude to my parents U Abdul Salam and Zainaba, for their unparalleled and unconditional support throughout my life. My brothers Reza

and Waazim, have been a real source of inspiration. The amount of joy they get from my successes, I am yet to fathom.

Finally, I am most grateful for the support from my lovely wife, Rahina. Rahi, your understanding and patience made this effort possible.

ABSTRACT

Author :	Zaqie Reza
Title:	Dissipation and Eddy Mixing Associated with Flow Past an Underwater Turbine
Institution:	Florida Atlantic University
Thesis Advisor:	Dr Manhar Dhanak
Degree:	Master of Science
Year:	2010

The objective of this thesis is to analyze the flow past an ocean current turbine using a finite volume Navier-Stokes CFD solver. A full 3-D RANS approach in a moving reference frame is used to model the flow. By employing periodic boundary conditions, one-third of the flow-field is analyzed and the output is replicated to other sectors. Following validation of the computation with an experimental study, the flow fields and particle paths for the case of uniform and sheared incoming flows past a generic turbine with various blade pitch angles are evaluated and analyzed. Flow field and wake expansion are visualized. Eddy viscosity effects and its dependence on flow field conditions are investigated.

DISSIPATION AND EDDY MIXING ASSOCIATED WITH FLOW PAST AN UNDERWATER TURBINE

LIST OF FIGURES

1. INTRODUCTION

1.1 The Gulf Stream

The Gulf Stream is one of the world's most intensively studied current systems. It is a powerful, warm and swift current which originates in Gulf of Mexico exits through the Straits of Florida and flows though the east coast of the United States of America all the way till Cape Hatteras, North Carolina. After this point the stream ceases to keep a steady path. It cuts across North Atlantic, passing through south of the Grand Banks and the waves meander. At around east of 60°W, the Gulf Stream ceases to be a single well defined stream and branches out. It shifts north in the fall and while in winter and early spring it shifts south. It is a geostrophic system, i.e. the pressure gradient force balances the Coriolis force (Stommel, [1]).

The width of the surface of the Gulf Stream is between 100 and 150 km and the surface velocities of the Gulf Stream can reach up to 2.5 m/s (Knauss, [2]). The Florida current along the southern and eastern shores of Florida amount to 20% of the Gulf Stream. It has a mass flow 30 times greater than total fresh water river flows of the world and total energy flux of 20 GW(Hanson et al, [3]). Obviously, the kinetic energy of such a stream has significant potential to supply Florida with much of its needed consumer electricity, provided that technically-feasible and environmentally-friendly harvesting technology can be developed.

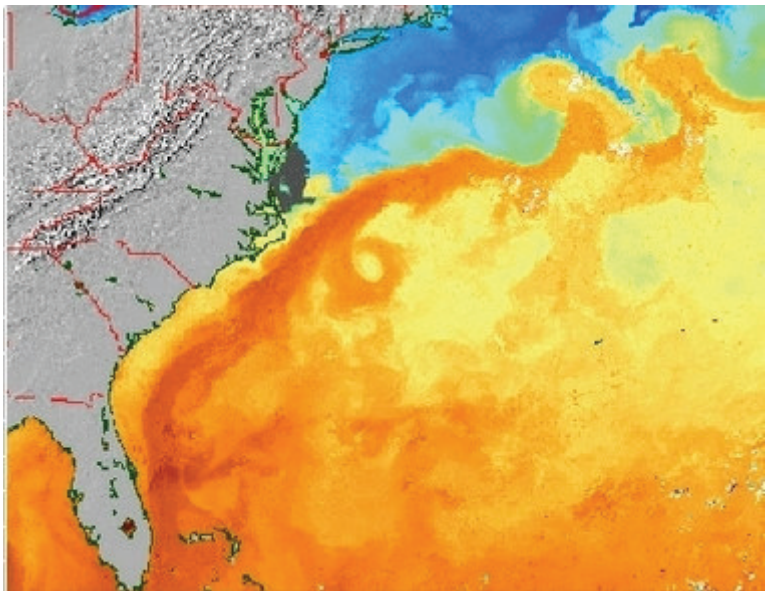

Figure (1) A geographical representation of the Gulf Stream (NASA, [4])

Pictured above in figure (1) is the East Coast of the United States, in grey, with the Gulf Stream, in orange, revealed through Sea Surface Temperature data (SST).

Although harnessing the energy of the Gulf Stream has been considered for over a century, no system has been installed for more than a few hours. Therefore, no technical or environmental knowledge-base exists for in-situ operation, from which to design turbines, or make decisions for policy and permitting. Hence FAU's Center for Ocean Energy Technology (COET) intends to install a small-scale experimental ocean current turbine offshore South Florida (COET, [5]).

1.2 Energy Scenario in Florida

Even though energy situation in Florida is not grave situation at this moment of time, the state is destined for serious crises in energy needs in immediate future. Work done by COET elaborated on the necessities of the state and electricity generation potential of the

of the gulf stream (COET, [5][6]).

The electricity consumption in the state has increased by 3.8% per year and it is estimated to increase by 30% in the next ten years. To sustain this energy demand, Florida will need to increase its energy production capacity by 17000 Megawatts (MW). Currently the state is majorly reliant on non renewable source of energy such as natural gas, coal and other fossil fuels. A part of the energy also comes from nuclear fuel. This reliance on out of state petroleum industry being considerable makes state of Florida vulnerable to the volatility of the industries supply interruptions and price increases. For example the electricity cost has increased by more than 50% since 2000.

At present only 2% accounts for instate renewable energy in Florida. Hence the state is looking for alternatives to hydrocarbon based energy. Ocean energy has a great potential to provide much of Florida's energy needs.

Florida is an ideal location to develop this technology. Florida is a peninsula with the longest coastline in the continental United States, nearly 1400 miles of general coastline, almost 8500 miles of tidal shoreline, and with over 70% of its population living within 10 miles of the coast. Gulf Stream is hence a potential source of energy for the state.

1.3 Ocean Current Energy v/s Other Renewable Sources

The relatively constant flow of the ocean currents like the Gulf Stream, Peru Current or California Current carries large amount of energy that if used wisely can be utilized for power generation. Ocean currents flow patterns are the result of effects of the wind, water salinity and temperature, topography of the ocean floor, and the earth's rotation. These

currents, in contrast to tidal currents near the shore are relatively constant and flow in one direction only.

In comparison to wind energy, ocean currents carry a large amount of energy. This is because the density of water is about 830 times that of wind. So for a given surface area water speed of 1m/sec produces a similar amount of power as a constant wind speed of 10m/sec. Also, ocean currents are continuous and predictable in nature. Therefore unlike most other renewable source of energy, the future availability can be known and planned for. The resource is abundant and can be exploited with very little environmental impact (OCS, [7]).

1.4 Motivation

The conversion of kinetic energy to electrical energy from ocean currents offers exciting proposition as mentioned in the earlier sections. The majority of work done on such kind of analysis is based on horizontal axis wind turbine. Even though most of technology can be learnt and borrowed from wind turbine analysis, there lie few significant differences. These include the effect of free surface, effect of viscosity and possible occurrence of cavitation.

At present, design of turbines are based on the fundamental coefficient of power equation given by

$$C_P = \frac{P}{1/2\,\rho U_0^3 A} \qquad [1.1]$$

Where P is the power extracted by the turbine, ρ the density of water, U_0 is the free stream velocity and A the actuator disk area.

This equation is analogous to that in wind turbines. And it has a theoretical maximum with a value

$$C_{p\,max} = 0.593 \qquad [1.2]$$

This is called the Betz limit. The limit is also sometimes called as Lanchester–Betz–Joukowsky limit (Kuik,[8]). Numerous experimental and numerical calculations have shown that the Betz limit is being followed, especially for wind turbines.

There is a general consensus on the value of Betz limit. But there are some research which says power extracted by a turbine could more than that estimated by actuator disk theory and Betz limit. One such work was done can be found in the work done by Xiros (Xiros, [9]), where the authors state that axial force and absorbed force are underestimated by a large amount if the expansion of wake is large leading to higher values of C_p. However this has not been validated experimentally yet.

Because the concept of underwater turbines is a relatively new one, the amount of literature on their analysis available is few. Bahaj and et al (Bahaj,[10][11][12]) has pioneered in experimental testing of a turbine which is the proving ground for validation of this thesis.

The research by the group focuses on cavitation tunnel and tank tests on a marine current turbine (MCT). Validation of the CFD code is derived from the comparison with experimental measurements conducted on a model 800mm diameter turbine in a cavitation tunnel and a towing tank. The group conducted studies on the turbine with varying tip immersion, flow velocities, yaw angles and cavitation tests. The experimental data in [11] includes measurements of shaft power of the turbine for a series of blade pitch settings and speeds, in a non dimensionalised format with Tip Speed Ratio(TSR) v/s C_p values charts.

The numerical methods employed in analysis can be mainly sorted into two

- Potential flow methods.
- Reynolds Averaged Navier Stokes (RANS) methods

Potential flow method currently used can be divided as follows

- The momentum method
- The boundary-element method
- The blade element method
- The finite element method
- Discrete vortex method
- Vortex lattice method

The momentum method (Camporeale, [13]) and the boundary element method (Calcagno, [14]) is used to predict the power output from a turbine, the blade element method[] can be used to predict the force on the blade on the turbine. The finite element methods have been used to predict the wake of the turbine (Ponta, [15]). Vortex lattice method (Goly, [16]) can be used to measure pressure on the blade and the power extracted by a turbine.

Discrete vortex method (Li, [17]) is used to predict power output and the wake of a turbine.

RANS methods can predict the performance of turbines with high accuracy with very fine and good quality meshes. Because of the mesh requirements, the computational cost involved is very high. Nevertheless, the amount of data that can be collected and the extend of comprehensiveness of the approach make it a luring method for analysis of any fluid related problems. RANS methods for flow involving turbines are based on solving the fundamental equations for conservation of mass and balance of momentum. RANS models have been widely employed for wind turbine anaylsis. Carcangiu (Carcangiu, []) have done an extensive study on horizontal axis wind turbine using ANSYS Fluent.

1.4 Scope of the Thesis

The plan to install many turbines (on a commercial scale) in the Gulf Stream has lead to doubts regarding large scale impact of the turbines on the Gulf Stream itself. Researchers at Florida State University (FSU) are looking at modeling the Atlantic Basin and the North Atlantic Circulation to consider the question. Their computation involves a grid of 0.5 x 0.5 km in the horizontal plane and requires some representation of the presence of operating turbines within the grid.

In the present work a RANS flow model of an ocean current turbine is validated against an experimental data and a flow visualization study is carried out. An attempt to visualize wake expansion is done. A comparison on the velocity profiles for different hub pitch angles at different sections of the control volume is performed. A study of the flow

with a shearing velocity profile is carried out and a comparison with uniform flow is conducted.

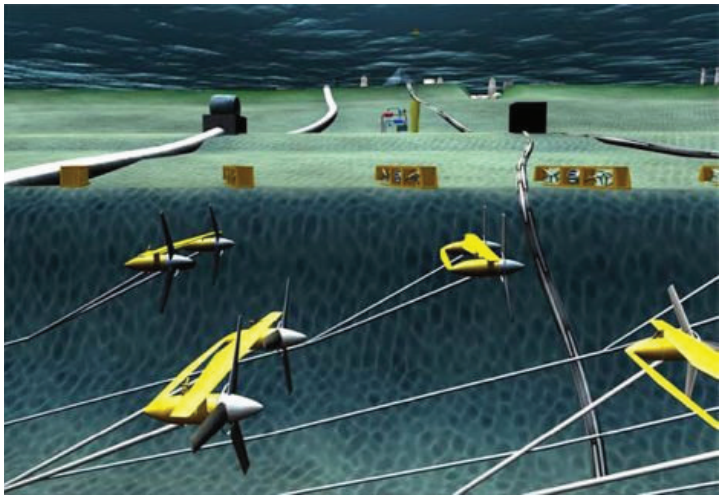

Figure (2) Graphic representation of the ocean current turbines in the Gulf Stream (COET, [5])

2. COMPUTATIONAL FLUID DYNAMICS

Computational Fluid Dynamics (CFD) can be explained as numerical solution of the differential governing equations of fluid flows, with the help of computers. Any CFD program is based on solution to any of the three fundamental principles:

- Conservation of mass
- Newtons second law
- Conservation of energy

These fundamental principles can be expressed in terms of mathematical equations, mostly integral or partial derivatives. CFD is the art of replacing these equations with discretised algebraic forms, which in turn are solved to obtain results in form of numbers for the flow field values at discrete points in space and time. Hence the end product of CFD simulation is a collection of numbers(Anderson, [18]).

2.1 Advantages of CFD

CFD has a lot of advantages over conventional methods of analysis

1. It is faster than traditional approaches. And with software like Fluent a lot of various parameters can be varied and checked without any loss of time.It is difficult to model tests for all the systems that are to be checked. Hence a validated CFD code can be used to run a simulation on a model similar to the model which was used for validation.

2. CFD solutions can be got with good accuracy if done with proper inputs.
3. With the latest advancements in CFD, solution can be analyzed effectively at every location and any time instant of the model with ease.
4. With the latest advancements in technology and newer mathematical formulations and solution schemes, the models give good accuracy, making experiment redundant in many cases.
5. And with latest advanced personal computers and faster algorithms in the CFD packages it is possible to the analysis without the use of heavily configured computers.

2.2 The CFD code

The CFD code can be divided into three phases: Preprocessor, Solver and Post Processing.

2.2.1 Preprocessor

Pre processor is the starting point for a CFD problem. In this phase the problem is implemented into a mathematical model. Various processes in preprocessor are:

- Creating geometry
- Creation of descretised models by grid or mesh generation
- Setting of loads and boundary conditions
- Setting of solver parameters.

The domain is defined and subdivided into smaller portions called *grid* or *mesh*. The boundary conditions are set. Since the CFD solution depends locally on the properties of meshes, meshing is a very important part of the process. Greater the number of meshes

greater is the accuracy. Also mesh spacing has to be enhanced (fine mesh size) near region of high variable gradients and coarse where there is smooth changes in the flow. Also quality of mesh and type of mesh affects the result to a great deal. Effect of mesh type on the calculations is explained later. The final success of a CFD simulation depends on the Preprocessing.

2.2.2 Solver

The numerical solution algorithm is the core of CFD code. CFD solvers work with the following procedure

- The problem is modeled using simple analytical functions.
- The governing equations are discretised for the mesh and its resolution.
- The algebraic system of equations is solved.

2.2.3 Post Processing

It includes the analysis and understanding of the results. A sound understanding of the various terminologies and their anticipated values is required so that the result can make sense. The results can include vectors, contours, line plots, particle tracks etc.

2.3 The software FLUENT

2.3.1 Finite-Volume approach

The commercial code Fluent solves the governing integral equations for the conservation of mass and momentum, and (when appropriate) for energy and other scalars, such as turbulence and chemical species. In both cases a control-volume-based technique is used, which consists of:

- Division of the domain into discrete control volumes using a computational grid.
- Integration of the governing equations on the individual control volumes to construct algebraic equations for the discrete dependent variables (unknowns), such as velocities, pressure, temperature, and conserved scalars.
- Linearisation of the discretised equations and solution of the resultant linear equation system, to yield updated values of the dependent variables.

Fluent is a commercial 2D/3D unstructured mesh solver, which adopts multigrid solution algorithms. It uses a co-located grid, meaning that all flow parameters are stored in the cell-centres. Processes can be easily parallelised on multiple computer nodes.

Two numerical methods are available in Fluent:

- Pressure-based solver
- Density-based solver

The first one was developed for low-speed incompressible flows, whereas the second was created for the high-speed compressible flows solution. In the present study, which involves incompressible flows, the pressure-based approach was used.

2.3.2 The pressure-based solver

The pressure-based solver employs an algorithm which belongs to a general class of methods called the projection method. In the projection method, the constraint of mass conservation (continuity) of the velocity field is achieved by solving a pressure (or pressure correction) equation. The pressure equation is derived from the continuity and the momentum equations in such a way that the velocity field, corrected by the pressure,

satisfies the continuity. Since the governing equations are nonlinear and coupled to one another, the solution process involves iterations wherein the entire set of governing equations is solved repeatedly until the solution converges.

Two types of solution algorithms are available in Fluent:

- Segregated
- Coupled

The segregated pressure-based solver uses a solution algorithm where the governing equations are solved sequentially (i.e. segregated) from one another. The segregated algorithm is memory-efficient, since the discretized equations need only be stored in the memory one at a time. However, the solution convergence is relatively slow, in as much as the equations are solved in a decoupled manner.

The pressure-based coupled algorithm solves a coupled system of equations comprising the momentum equations and the pressure-based continuity equation. The remaining equations (i.e. scalars) are solved in a decoupled fashion as in the segregated algorithm. Since the momentum and continuity equations are solved in a closely coupled manner, the rate of solution convergence significantly improves when compared to the segregated algorithm. However, the memory requirement increases by 1.5 - 2 times that of the segregated algorithm since the discrete system of all momentum and pressure-based continuity equations needs to be stored in the memory when solving for the velocity and pressure fields (rather than just a single equation, as is the case with the segregated algorithm).

2.3.3 Pressure-Velocity Coupling

Solution of Navier-Stokes equation is complicated because of the lack of an independent equation for the pressure, whose gradient contribute to each of the three momentum equations. Moreover, for incompressible flows, the continuity equation does not have a dominant variable, but it is rather a kinematic constraint on the velocity field. Thus, the pressure field (the pressure gradients when incompressible) should be generated by satisfying mass conservation. Several approaches for pressure-velocity coupling are possible, like SIMPLE, SIMPLEC, PISO and Coupled. Coupled scheme has been used in this thesis. The pressure based coupled algorithm obtains a more robust and efficient single phase implementation for steady-state flows.

3. FORMULATION

3.1 Governing Equations

The study of any fluid dynamics problems are based on the fundamental mass, momentum and energy conservation principles (FLUENT, [19]). The governing equations are as follows:

3.1.1 Continuity Equation

The equation of conservation of mass, or continuity equation, can be written as follows

$$\frac{d\rho}{dt} + \nabla.(\rho\vec{v}) = S_m \qquad [4.1]$$

Where ρ is the density of the fluis and $\vec{v}$ is the velocity vector. The source S_m is the mass added to the continuous phase from the dispersed second phase, e.g. due to vaporization of liquid droplets high temperature simulations.. S_m is zero in this problem as there is no change in phase.

3.1.2 The Momentum Balance Equation

The equation for balance of momentum

$$\frac{d}{dt}(\rho\vec{v}) + \nabla.(\rho\vec{v}) = -\nabla p + \nabla.\bar{\bar{\tau}} + \rho\vec{g} + \vec{F} \qquad [4.2]$$

Where p is the static pressure, and $\rho\vec{g}$ and $\vec{F}$ are the gravitational body force and external body forces (e.g., that arise from the interaction with the dispersed phase), respectively. $\vec{F}$ also contains other model-dependent source terms such as porous-media and user-defined sources.

The stress tensor $\bar{\bar{\tau}}$ is given by

$$\bar{\bar{\tau}} = \mu[(\nabla\vec{v} + \nabla\vec{v}^{T}) - \frac{2}{3}\nabla.\vec{v}I] \quad [4.3]$$

Where μ is the molecular viscosity, I is the unit tensor, and the second term on the right hand side is the effect of volume dilation.

3.2 Rotating Reference Frames

The principal reason for employing a moving reference frame is to render a problem which is unsteady in the stationary (inertial) frame, steady with respect to the moving frame. For a steadily rotating frame (i.e., the rotational speed is constant), it is possible to transform the equations of fluid motion to the rotating frame such that steady-state solutions are possible. A rotating rotor of a water turbine is such case. With a moving reference frame, the flow around the moving part can be modeled (with certain restrictions) as a steady-state problem, with respect to the moving frame. When a moving reference frame is activated, the equations of motion are modified to incorporate the additional acceleration terms which occur due to the transformation from the stationary to the moving reference frame. By solving these equations in a steady-state manner, the flow around the moving parts can be modeled.

3.3 Relative Velocity Formulation

Consider a coordinate system which is rotating steadily with angular velocity $\vec{\omega}$ relative to a stationary (inertial) reference frame (See figure(2)). The origin of the rotating system is located by a position vector $\vec{r}_o$.

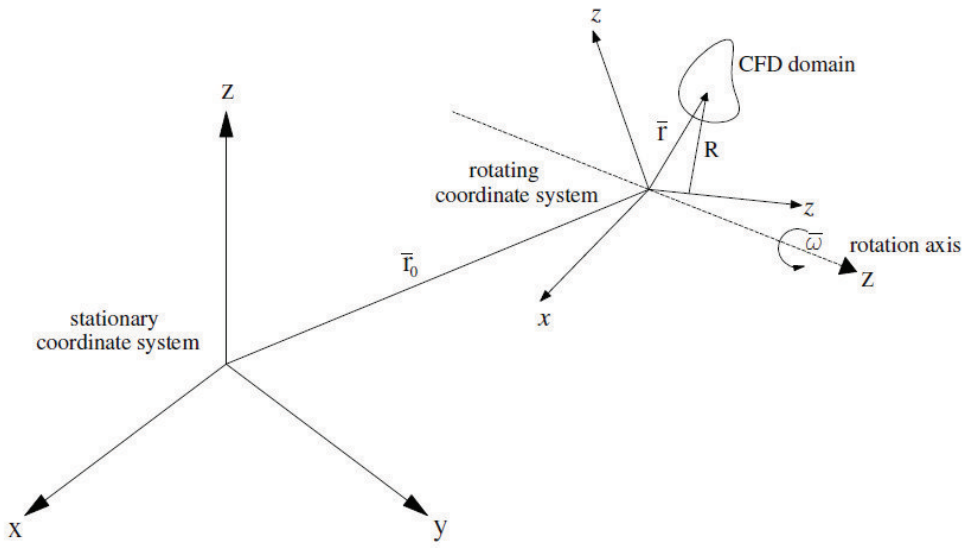

Figure(3) Coordinate system for moving frame of reference

The fluid velocities can be transformed from the stationary frame to the rotating frame using the following relations

$$\overrightarrow{v_r} = \vec{v} - \overrightarrow{u_r} \qquad [4.4]$$

$$\overrightarrow{u_r} = \vec{\omega} \times \vec{r} \qquad [4.5]$$

where $\vec{v}_r$ is the relative velocity (the velocity viewed from the rotating frame), $\vec{v}$ is the absolute velocity (the velocity viewed from the stationary frame), and $\vec{u}_r$ is the whirl velocity(the velocity due to the moving frame).

For the relative velocity formulation, the governing equations of fluid flow for a steadily rotating frame can be written as follows:

Conservation of mass:

$$\frac{\partial \rho}{\partial x} + \nabla . (\rho \overrightarrow{v_r}) = 0 \qquad [4.6]$$

Balance of momentum:

$$\frac{\partial}{\partial x}(\rho \overrightarrow{v_r}) + \nabla . (\rho \vec{v}_r \vec{v}_r) + \rho(2\overrightarrow{\omega} \times \vec{v}_r + \overrightarrow{\omega} \times \overrightarrow{\omega} \times \vec{r}) = -\nabla p + \nabla . (\bar{\bar{\tau}}_r) + \vec{F} \qquad [4.7]$$

The momentum equation contains two additional acceleration terms: the Coriolis acceleration $2\overrightarrow{\omega} \times \vec{v}_r$ and the centripetal acceleration $\overrightarrow{\omega} \times \overrightarrow{\omega} \times \vec{r}$.

3.4 Turbulence Modeling

Turbulent flows are characterized by fluctuating velocity fields. These fluctuations mix transported quantities such as momentum, energy, and species concentration, and cause the transported quantities to fluctuate as well. Since these fluctuations can be of small scale and high frequency, they are computationally expensive to simulate directly in practical engineering calculations. Instead, the instantaneous (exact) governing equations

can be time-averaged, ensemble-averaged, or otherwise manipulated to remove the resolution of small scales, resulting in a modified set of equations that are computationally less expensive to solve. However, the modified equations contain additional unknown variables, and turbulence models are needed to determine these variables in terms of known quantities.

3.5 Reynolds-Averaged Approach and Filtering

Time-dependent solutions of the Navier-Stokes equations for high Reynolds-number turbulent flows in complex geometries which set out to resolve all the way down to the smallest scales of the motions are very difficult to attain. Two alternative methods can be employed to render the Navier-Stokes equations tractable so that the small-scale turbulent fluctuations do not have to be directly simulated:

- Reynolds-averaging (or ensemble-averaging)
- Filtering

Both methods introduce additional terms called as *closure terms* in the governing equations that need to be modeled to get a solution.

3.5.1 Reynolds-averaged Navier-Stokes (RANS)

The Reynolds-averaged Navier-Stokes (RANS) equations govern the transport of the averaged flow quantities, with the whole range of the scales of turbulence being modeled. The RANS-based modeling approach therefore greatly reduces the required computational effort and resources. The RANS equations are often used to compute time-dependent flows, whose unsteadiness may be externally imposed (e.g., time-dependent

boundary conditions or sources) or self-sustained (e.g., vortex-shedding, flow instabilities).

In Reynolds averaging, the solution variables in the instantaneous (exact) Navier-Stokes equations are decomposed into the mean (ensemble-averaged or time-averaged) and fluctuating components. For the velocity components

$$u_i = \bar{u}_i + u_i' \qquad [4.8]$$

Where $\overline{u_i}$ and u'_i are the mean and fluctuating velocity components (i = 1, 2, 3).

Likewise, for pressure and other scalar quantities:

$$\Phi = \bar{\Phi} + \Phi' \qquad [4.9]$$

where Φ denotes a scalar such as pressure, energy, or species concentration.

Substituting expressions of this form for the flow variables into the instantaneous continuity and momentum equations and taking a time (or ensemble) average (and dropping the overbar on the mean velocity) yields the ensemble-averaged continuity and momentum equations. They can be written in Cartesian tensor form as:

$$\frac{\partial \rho}{\partial x} + \frac{\partial}{\partial x_i}(\rho u_i) = 0 \qquad [4.10]$$

$$\frac{\partial}{\partial t}(\rho u_i) + \frac{\partial}{\partial x_j}(\rho u_i u_j) = -\frac{\partial \rho}{\partial x_i} + \frac{\partial}{\partial x_j}\left[\mu\left(\frac{\partial u_i}{\partial x_j} + \frac{\partial u_j}{\partial x_i} - \frac{2}{3}\delta_{ij}\frac{\partial u_i}{\partial x_j}\right)\right] + \frac{\partial}{\partial x_j}\left(-\rho\overline{u_i' u_j'}\right) \qquad [4.11]$$

Equations (3.10) and (3.11) are called Reynolds-averaged Navier-Stokes (RANS) equations. They have the same general form as the instantaneous Navier-Stokes

equations, with the velocities and other solution variables now representing ensemble-averaged (or time-averaged) values. Additional terms now appear that represent the effects of turbulence i.e the Reynolds stresses, $-\rho\overline{u_i' u_j'}$. Just as the transfer of momentum by collision is modeled in terms of velocity gradients and coefficient of viscosity, the Reynolds-stress components are modeled in terms of mean velocity and turbulent (or eddy) viscosity coefficients.

The eddy viscocity coefficients can be determined only numerically or through simulation of particular flow. This is where different models come in handy.

There are two approaches to RANS models

- Boussinesq hypothesis
- Reynolds stress transport models

Boussinesq Approach

The Reynolds-averaged approach to turbulence modeling requires that the Reynolds stresses in equation (3.11) are appropriately modeled. A common method employs the Boussinesq hypothesis to relate the Reynolds stresses to the mean velocity gradients:

$$-\rho\overline{u_i' u_j'} = \mu_t\left(\frac{\partial u_i}{\partial x_j} + \frac{\partial u_j}{\partial x_i}\right) - \frac{2}{3}\left(\rho k + \mu_t \frac{\partial u_k}{\partial x_k}\right)\delta_{ij} \qquad [4.12]$$

The Boussinesq hypothesis is used in the k-ε, Spalart-Allmaras model and the k-ω models. The advantage of this approach is the relatively low computational cost associated with the computation of the turbulent viscosity,μ_t. In the case of the Spalart-Allmaras model, only one additional transport equation (representing turbulent viscosity)

is solved. The advantage of this approach is the relatively low computational cost associated with the computation of the turbulent viscosity,$\mu_{t.}$ The disadvantage of the Boussinesq hypothesis is that it assumes μ_t as an isotropic scalar quantity, which is not true in actual sense.

Reynolds Stress Transport Models

RSM solves transport equations for each of the terms in the Reynolds stress tensor. An additional scale-determining equation (normally for ε) is also required. The hypothesis for isotropic eddy-viscosity is abandoned. This means that five additional transport equations are required in 2D flows and seven additional transport equations must be solved in 3D.

In many cases, models based on the Boussinesq hypothesis perform very well, and the additional computational expense of the Reynolds stress model is not justified. However, the RSM is clearly superior in situations where the anisotropy of turbulence has a dominant effect on the mean flow. Such cases include highly swirling flows and stress-driven secondary flows.

3.5.2 Filtering

Large Eddy Simulation (LES) is a type of filtering. Turbulent flows are characterized by eddies with a wide range of length and time scales. The largest eddies are typically comparable in size to the characteristic length of the mean flow. The smallest scales are responsible for the dissipation of turbulence kinetic energy. In LES, large eddies are resolved directly, while small eddies are modeled.

3.6 Model Selected

The RANS model selected for this thesis is Standard k-ε with standard wall functions (see chapter 5 for details on near wall mesh resolution).

The K-epsilon model is one of the most common turbulence models. It is a two equation model that means, it includes two extra transport equations to represent the turbulent properties of the flow. The first transported variable is turbulent kinetic energy, k. The second transported variable in this case is the turbulent dissipation, ε. It is the variable that determines the scale of the turbulence, whereas the first variable, k, determines the energy in the turbulence.

Robustness, economy, and reasonable accuracy for a wide range of turbulent flows explain its popularity in industrial flow and heat transfer simulations. It is a semi-empirical model, and the derivation of the model equations relies on phenomenological considerations and empiricism.

The standard – model (Launder and Spalding, [20]) is a semi-empirical model based on model transport equations for the turbulence kinetic energy (k) and its dissipation rate (ε). The model transport equation for k is derived from the exact equation, while the model transport equation for ε was obtained using physical reasoning and bears little resemblance to its mathematically exact counterpart.

In the derivation of the k - ε model, the assumption is that the flow is fully turbulent. It has been modified by the use of standard wall functions to capture the effect of wall (turbine) for the purpose of this thesis.

Transport Equations for the Standard k- ε Model

The turbulence kinetic energy, k , and its rate of dissipation, ε, are obtained from the following transport equations:

$$\frac{\partial}{\partial t}(\rho k) + \frac{\partial}{\partial x_i}(\rho k u_i) = \frac{\partial}{\partial x_j}\left[\left(\mu + \frac{\mu_t}{\sigma_k}\right)\frac{\partial k}{\partial x_j}\right] + G_k + G_b - \rho\varepsilon - Y_M + S_k \quad [4.13]$$

$$\frac{\partial}{\partial t}(\rho\varepsilon) + \frac{\partial}{\partial x_i}(\rho\varepsilon u_i) = \frac{\partial}{\partial x_j}\left[\left(\mu + \frac{\mu_t}{\sigma_\varepsilon}\right)\frac{\partial \varepsilon}{\partial x_j}\right] + C_{1\varepsilon}\frac{\varepsilon}{k}(G_k + C_{3\varepsilon}G_b) - C_{2\varepsilon}\rho\frac{\varepsilon^2}{k} + S_\varepsilon \quad [4.14]$$

where,

G_k	=	turbulence kinetic energy due to mean velocity gradients
G_b	=	turbulence kinetic energy due to buoyancy
Y_M	=	contribution of fluctuating dilation in compressible turbulence to overall dissipation rate
$C_{1\varepsilon}, C_{2\varepsilon}, C_{3\varepsilon}$	=	experimentally determined constants
$\sigma_k, \sigma_\varepsilon$	=	experimentally determined turbulent Prandtl numbers for k and ε
S_k, S_ε	=	source terms

The turbulent viscosity is computed as

$$\mu_t = \rho C_\mu \frac{k^2}{\varepsilon} \quad [4.15]$$

where C_μ is a constant.

3.7 Boundary Conditions

The various boundary conditions used are as follows

- Velocity inlet – at domain inlet
- Outflow – at domain outlet

- Symmetry – domain extends
- Wall – water turbine
- Periodic boundary

The boundary conditions and their properties are as explained below.

Velocity Inlet

Velocity inlet boundary conditions are used to define the flow velocity, along with all relevant scalar properties of the flow, at flow inlets. The total pressure is not fixed but will rise to whatever value is necessary to give the necessary velocity distribution. In Fluent this boundary condition is intended for incompressible flows and it has to be kept as far away from a solid obstruction as possible.

When a velocity inlet boundary condition is defined, Fluent computes the mass flow rate, $\dot{m}$ as

$$\dot{m} = \int \rho \vec{v}.\, d\vec{A} \qquad [4.16]$$

Outflow

Outflow boundary conditions are used to model flow exits where the details of the flow velocity and pressure are not known prior to solving the flow problem. The solver extrapolates the required information from the interior. This boundary condtion is appropriate where the exit flow is close to fully developed condition. It assumes that there is a zero streamwise pressure gradient for all flow variables except pressure.

Symmetry

Symmetry boundary conditions are used when the physical geometry of interest, and the expected pattern of the flow/thermal solution, has mirror symmetry. They can also be used to model zero-shear slip walls in viscous flows as is the case with the problem at hand. In such cases the domain extend is kept to be at a distance as far as possible from the wall (turbine), so that there is little effect of boundary on the flow.

The properties of symmetry boundary conditions are as follows

- Zero flux of all quantities across a symmetry boundary.
- There is no convective flux across a symmetry plane: the normal velocity component at the symmetry plane is thus zero.
- There is no diffusion of flux across a symmetry plane: the normal gradients of all flow variables are thus zero at the symmetry plane

Wall

Wall boundary conditions are used to bound fluid and solid regions. The wall condition can used to model slip and non slip boundary conditions. It can be used at places where symmetry is used as zero shear slip walls.

The turbine is modeled as a no slip wall in the thesis.

Periodic

Periodic boundary conditions are used when the physical geometry of interest and the expected pattern of the flow/thermal solution have a periodically repeating nature. By using a periodic boundary, a part of the control volume need only be modeled, hence reducing the number of grids to a great extend.

Given below are figures depicting the boundary conditions used

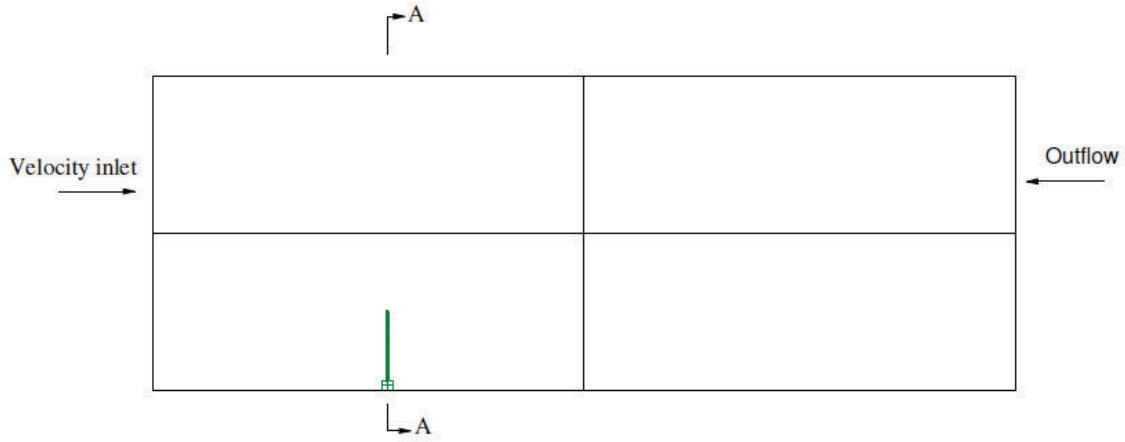

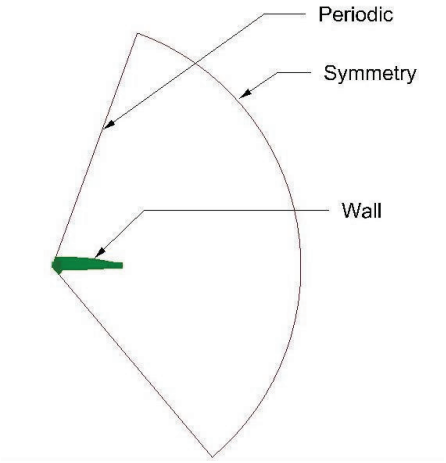

Section A

Figure (4) Applied boundary conditions

4. TURBINE CHARACTERISTICS AND FUNCTIONING

4.1 Hydrofoil Terminology

A number of terms are used to characterize an airfoil. The mean camber line is the locus of points midway between upper and lower surfaces of the airfoil. The most forward and rear ward end of this locus line is the leading edge and the trailing edge respectively. The line connecting the leading edge and the trailing edge is the chord line and the distance between the two edges is called chord, c. Camber is the distance from the mean camber line to the chord line, measured perpendicular to the chord line. The thickness t, is the distance between the upper and lower surfaces, also measured perpendicular to the chord line. The angle of attack, α, is the angle between the relative water velocity and the chord line. A graphic representation of an airfoil section is as follows:

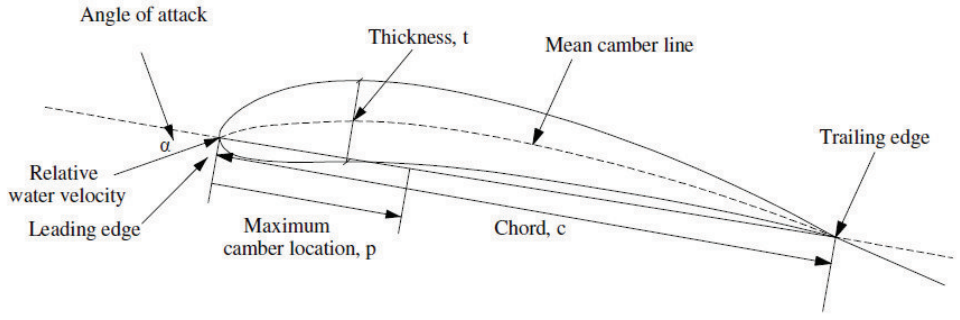

Figure (5) Foil section

4.2 Forces acting on an airfoil section

When an imminent flow encounters a foil section (as shown in figure (6)), forces act on it. The forces can be resolved as normal force, F_N , along the flow direction and thrust force orthogonal to it. Alternatively they can be resolved into lift force normal to the relative velocity of the flow and drag forces along the flow.

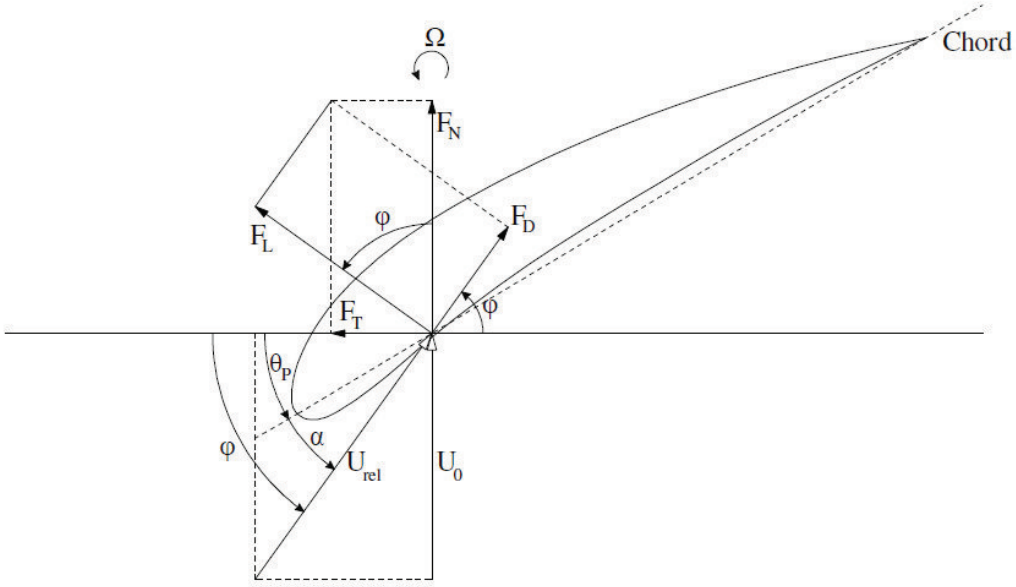

Figure (6) Forces acting on a hydrofoil

Where,

θ_P	=	Pitch angle
α	=	Angle of attack
φ	=	Angle of relative flow
U_0	=	Inflow velocity
U_{rel}	=	Relative velocity
Ω	=	Rotational velocity
F_L	=	Lift force
F_D	=	Drag force

F_N = Normal force

F_T = Thrust force

4.3 Basic Turbine Definitions

Tip Speed Ratio

The Tip Speed Ratio (TSR) is an important parameter for wind turbine design. It represents the ratio between the tip speed and the undisturbed wind speed.

$$\text{TSR} = \lambda = \frac{\Omega R}{U_0} \qquad [5.1]$$

where R is the radius of the wind turbine and **Ω** is the angular velocity of the rotor.

Thrust Coefficient

The thrust coefficient is ratio of thrust exerted on a turbine to maximum thrust that can exert on it. It is given by the expression:

$$C_T = \frac{T}{1/2\,\rho U_0^2 A} \qquad [5.2]$$

Power Coefficient

The power coefficient is ratio of power P extracted by the turbine to maximum power in the freestream. It is given by the expression:

$$C_P = \frac{P}{1/2\,\rho U_0^3 A} \qquad [5.3]$$

Explanation on C_P, its maximum possible value (Betz limit) and its derivation is explained later in this chapter.

Induction factors

The incoming flow is affected by the presence of rotor. The flow velocity at the blade is hence not equal to the water speed, but a reduced one. As given by the Actuator Disk Theory, axial induction factor, a is expressed as

$$a = \frac{U_0 - U_d}{U_0} \quad [5.4]$$

where U_d is the flow velocity at the disk or in other words flow velocity at the turbine.

The amount of axial induction factor decides the amount of power extracted by the turbine.

Lift and Drag Coefficients

Lift force (explained earlier) as calculated by Kutta and Joukowski is given by

$$L = \rho U_0 \Gamma \quad [5.5]$$

where Γ is the circulation or vortex strength of airfoil as defined as the integral

$$\Gamma = \oint uds \quad [5.6]$$

around any path s enclosing the airfoil and u is the tangential velocity to the path s.

Lift and drag coefficients define the characteristic of an airfoil

$$C_l = \frac{L}{0.5\rho U^2 c} \quad [5.7]$$

$$C_d = \frac{D}{0.5\rho U^2 c} \quad [5.8]$$

where L, D are forces per unit span, U the flow speed and c the chord length.

4.4 Turbine Power Production and Betz Limit

Power calculation for a wind turbine is explained extensively by Maxwell (Maxwell, [21]). The output power of a marine current turbine can be found out using the same principle and is governed by the equation:

$$P = \frac{1}{2}\rho A U^3 \quad [5.9]$$

Where ρ is the density, A the cross sectional area of the turbine and U the fluid stream velocity. However a turbine can only harness a fraction of this energy.

In actual case water turbine power production depends on the interaction between the rotor and the turbine. Power of a turbine can be determined by studying the forces generated by the mean water speed. By taking a simple actuator disk model one can get an estimate maximum possible power calculated on a turbine.

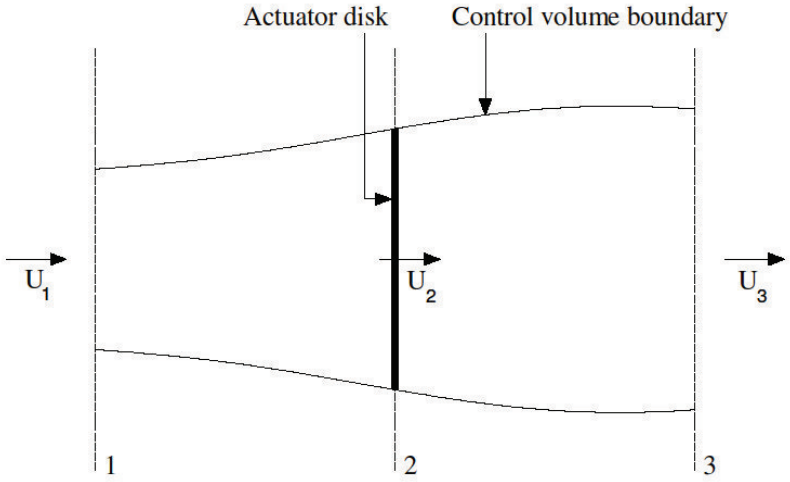

Figure(7) Actuator disk control volume

The assumptions for such an analysis can be as enlisted below,

- Homogenous, incompressible and steady state flow
- No frictional drag
- Infinite number of blades
- Uniform thrust over the disk or rotor area
- Non rotating wake
- Static pressure in the downstream and the upstream

A control volume is assumed with an actuator disk in the center (position 2) with position 1 as the inflow boundary and position 3 as the outflow boundary. By applying conservation of linear momentum the thrust is equal and opposite to the change in momentum of the air stream:

$$T = U_1(\rho AU)_1 - U_3(\rho AU)_3 \quad [5.10]$$

where ρ is the fluid density , A the area of cross-section of the actuator disk and U_1 and U_3 are the inflow and outflow velocity respectively. For a steady state flow $(\rho AU)_1$ and $(\rho AU)_3$ can be replaced by $\dot{m}$, where m is the mass flow rate. Then thrust becomes

$$T = \dot{m}(U_1 - U_3) \quad [5.11]$$

Across the disk the velocity is assumed to be same.

Applying Bernoulli function in the two control volumes

upstream:

$$p_1 + \frac{1}{2}\rho U_1^2 = p_{21} + \frac{1}{2}\rho U_2^2 \quad [5.12]$$

downstream:

$$p_{23} + \frac{1}{2}\rho U_2^2 = p_3 + \frac{1}{2}\rho U_3^2 \quad [5.13]$$

where p_{21} and p_{23} are pressure on the right and left side of the disk respectively. Pressures at far field p_1, p_3 are equal.

The thrust can be expressed as the net sum of the forces on each side of the actuator disk:

$$T = \frac{1}{2}\rho A(U_1^2 - U_3^2) \quad [5.14]$$

where A is the actuator disk area.

The thrust values from equation (4.11) and (4.14) when combined gives

$$U_2 = \frac{U_1 + U_3}{2} \qquad [5.15]$$

The power output, is equal to thrust times the velocity at the disk

$$P = \frac{1}{2}\rho A(U_1^2 - U_3^2) \cdot \left(\frac{U_1 + U_3}{2}\right) \qquad [5.16]$$

$$P = \frac{1}{4}\rho A U_1^3 \left(1 - \frac{U_3^2}{U_1^2}\right)\left(1 + \frac{U_3}{U_1}\right) \qquad [5.17]$$

For maximum power the term $\left(1 - \frac{U_3^2}{U_1^2}\right)\left(1 + \frac{U_3}{U_1}\right)$ should be maximum. Substituting x for $\frac{U_3}{U_1}$,

$$\frac{d}{dx}(1 - x^2)(1 + x) = 0$$

$$3x^2 + 2x - 1 = 0$$

From the above quadratic equation, $x = \frac{1}{3}$

Substituting for x in equation (5.17),

$$P_{max} = \frac{1}{4}\rho A U_1^3 \left(1 - \frac{1}{9}\right)\left(1 + \frac{1}{3}\right)$$

$$P_{max} = \frac{16}{27} \cdot \frac{1}{2}\rho A U_1^3 \qquad [5.18]$$

The coefficient of power C_P is defined by

$$C_P = \frac{\text{Rotor Power}}{\text{Power in the wind}} \quad [5.19]$$

Hence

$$C_{P\,max} = 0.5926$$

This is called that Betz Limit. It is the theoretical maximum possible power coefficient.

4.5 Turbine with rotating wake

For a rotating wind turbine, the flow behind the rotor rotates in the opposite direction to the rotor, in reaction to the torque exerted by the flow on the turbine. Because of this generation of rotational kinetic energy in the wake, lesser power is extracted by the turbine.

$C_{P\,max}$ for a turbine with wake rotation can be described as

$$C_{P\,max} = \frac{24}{\lambda^2}\int_{a_1}^{a_2}\left[\frac{(1-a)(1-2a)(1-4a)}{(1-3a)}\right]^2 da \quad [5.20]$$

where λ is the tip speed ratio a_1 and a_2 corresponds to axial induction factors at $\lambda_r = 0$ and $\lambda_r = \lambda$ respectively. The local tip speed ratio$\lambda_r = \frac{\lambda r}{R}$ (where r is the intermediate radius) is related to axial induction factor a as:

$$\lambda_r^2 = \frac{(1-a)(4a-1)^2}{1-3a} \quad [5.21]$$

When $\lambda_r = 0$, $a = a_1 = 0.25$ and when $\lambda_r = \lambda$, $a = a_2$. $a_2 = \frac{1}{3}$ is the upper limit of a_2 as evident from equation(4.21).

Figure(8) below gives a depiction of theoretical maximum power coefficient as a function of tip speed ratio with and without wake flow for a turbine.

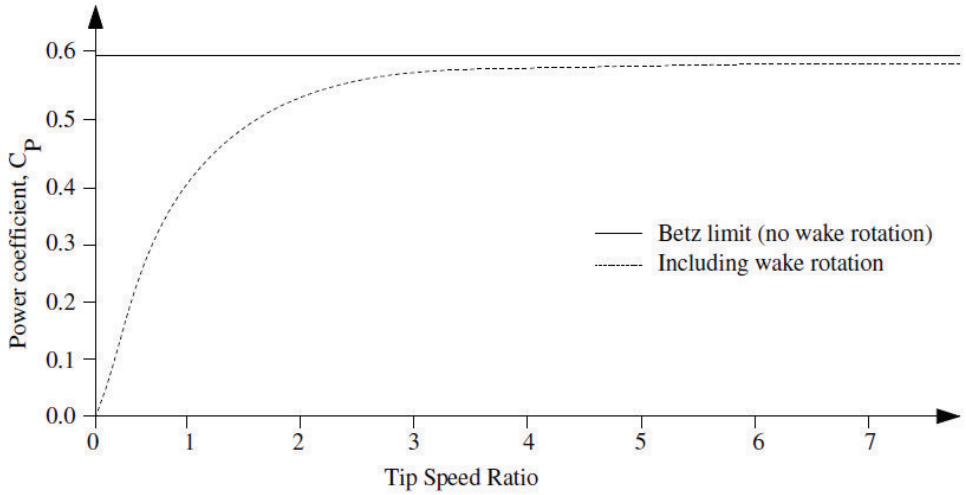

Figure (8) Cp curve for actuator disk with and without wake rotation

In practice, turbine blades are designed for optimum design tip speed ratio and then the performance of the turbine at all expected tip speed ratios are determined. $C_P - \lambda$ curves are one such performance curve. A combination of wind and rotor speed is used to vary the λ values. Given below is one such curve.

This thesis mainly focuses on analysis of one such turbine and its C_P characteristics for different kinds of flow. Also effect of eddy viscosity will be studied on the turbines power extraction capability.

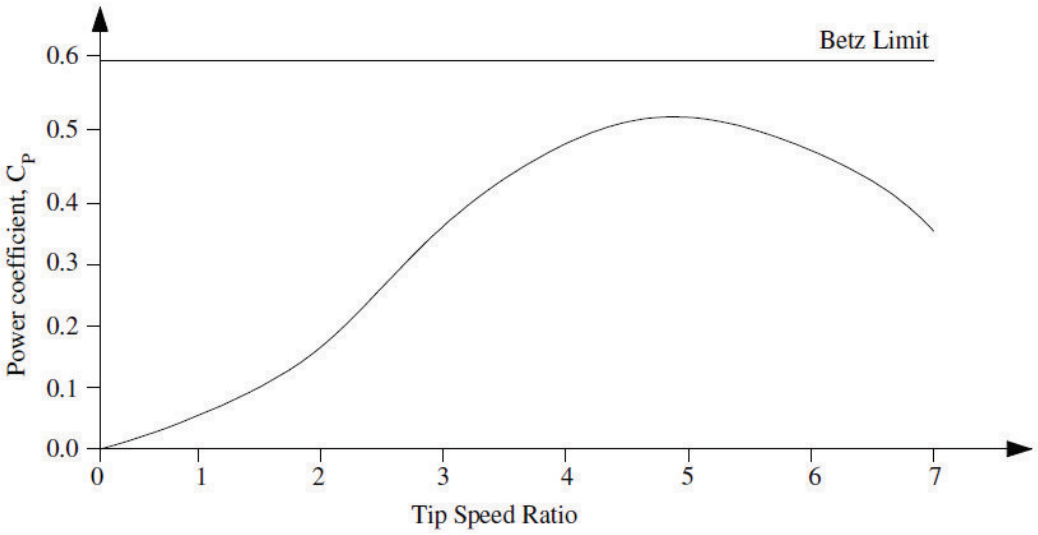

Figure (9) Cp curve for actual water turbine

There is a general consensus on the value of Betz limit. But there are some research which says power extracted by a turbine could more than that estimated by actuator disk theory and Betz limit. One such work was done can be found in the work done by Xiros (Xiros, [9]), where the authors state that axial force and absorbed force are underestimated by a large amount if the expansion of wake is large leading to higher values of C_p. However this have not be validated experimentally yet.

4.6 Blade and Hub Characteristic

The rotor used by Bahaj and group(Bahaj, [11]) is used for the entire analysis. NACA Five-Digit Series 638xx sections were used. The first digit when multiplied by 3/2, yields the design lift coefficient (C_l) in tenths. The next two digits, when divided by 2, give the position of the maximum camber (p) in tenths of chord. The final two digits indicate the maximum thickness (t) in percentage of chord. For example, NACA 63815 has a

maximum thickness of 15%, a design lift coefficient of 0.9, and a maximum camber located 19% back from the leading edge.

A blade radius of 3 meters and hub radius of 375 mm was considered. The particulars of turbine blade and hub are as listed below:

Main Particulars	
Rotor radius	3m
Blade length	2.625m
Hub radius	0.375m
Number of blades	3
Twist	15 degree
Foil Type	NACA 638xx

Table(1) Rotor particular

r/R	Radius r(mm)	c/R	Pitch Distribution(deg)	t/c(%)
0.2	600	0.125	15	24
0.25	750	0.1203	12.1	22.5
0.3	900	0.1156	9.5	20.7
0.35	1050	0.1109	7.6	19.5
0.4	1200	0.1063	6.1	18.7
0.45	1350	0.1016	4.9	18.1
0.5	1500	0.0969	3.9	17.6
0.55	1650	0.0922	3.1	17.1
0.6	1800	0.0875	2.4	16.6
0.65	1950	0.0828	1.9	16.1
0.7	2100	0.0781	1.5	15.6
0.75	2250	0.0734	1.2	15.1
0.8	2400	0.0688	0.9	14.6
0.85	2550	0.0641	0.6	14.1
0.9	2700	0.0594	0.4	13.6
0.95	2850	0.0547	0.2	13.1
1	3000	0.05	0	12.6

Table (2) Foil Section Characteristics

A graphic representation of the designed blade is as shown below:

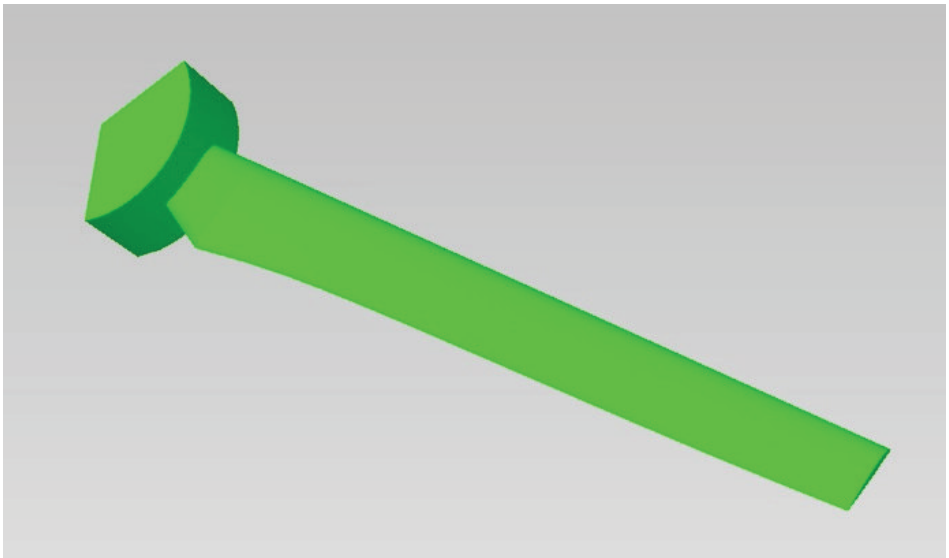

Figure(10) Designed blade

5. MESH GENERATION

Mesh generation is a time consuming and the most critical part of CFD simulation (Chmltech, [22]). The quality of the mesh plays a direct role in quality of the analysis. These types of mesh utilize quadrilateral elements in 2D and hexahedral elements in 3D in a computationally rectangular array.

Mesh can be classified into two categories

- Structured Mesh
- Unstructured Mesh
- Hybrid Mesh

5.1 Structured Mesh

Mesh is laid out in a regular repeating pattern called blocks. These types of mesh utilize quadrilateral elements in 2D and hexahedral elements in 3D in a computationally rectangular array. Although the element topology is fixed, the mesh can be shaped to be body fitted through stretching and twisting of the block.

Advantages of Structured Mesh

- Allows user a high degree of control.
- Quadrilateral and hexahedral elements, which are very efficient at filling space, support a high amount of skewness and stretching before the solution will be

significantly affected. This helps in condensing points in regions of high gradients and flowfield.

- The mesh can be easily flow direction oriented as mesh generation is done manually.
- Post processing of the results on a structured block mesh is typically a much easier task because the logical mesh planes make excellent reference points for examining the flow field and plotting results.

Disadvantages of structured mesh

- Structured mesh generation is time consuming.
- It requires a high degree of expertise. Often a good mesh generation is coherent with high degree of expertise and brute force placement of control points and edges.

5.2 Unstructured Mesh

Unstructured mesh utilize an arbitrary collection of elements to fill the domain. Because the arrangement of elements has no discernible pattern, the mesh is called unstructured. These types of mesh typically utilize triangles in 2D and tetrahedral in 3D.

Advantages of Structured Mesh

- They are automated and hence require little user time or effort.
- Require little user input and hence easier to generate
- Enables solution of very large and detailed problems in a relatively short period of time.

Disadvantages of Structured Mesh

- Lack of user control when laying out the mesh. Typically user control is limited to the boundaries of the mesh with the mesher automatically filling the interior.
- Requires good CAD data. Most meshing failures are due to some error in CAD model.

5.3 Hybrid Mesh

Hybrid mesh utilizes some form of structured mesh in local regions while using unstructured mesh in the bulk of the domain. Hybrid meshs can contain hexahedral, tetrahedral, prismatic and pyramid elements in 3D and triangles and quadrilaterals in 2D and triangles and quadrilaterals in 2D.

Advantages of Hybrid Mesh Methods

- Both structured and unstructured meshs can be used simultaneously at different locations as per the requirements.
- The shape and distribution of the mesh can be controlled locally.

Disadvantages of Hybrid Methods

- They can be difficult to use and require user expertise.
- Hybrid methods are less robust than unstructured methods.

Given below are the various mesh topologies that are commonly used.

5.4 Types of Elements and Their Properties

The types of elements that are used for mesh generation are: hexahedral, tetrahedral, prismatic and pyramid elements in 3D and triangles and quadrilaterals in 2D.

Hexahedral Elements

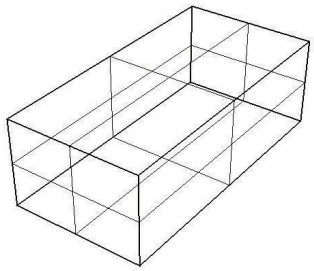

They are excellent near solid boundaries (where flow field gradients are high) and afford a user a high degree of control, but is time consuming to generate.

Prismatic Elements

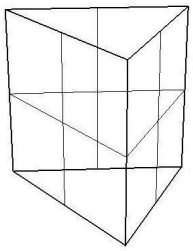

They are triangles extruded into wedges and are useful for resolving near wall gradients, but suffer from the fact that they are difficult to cluster in the lateral direction due to the underlying triangular structure.

Tetrahedral Elements

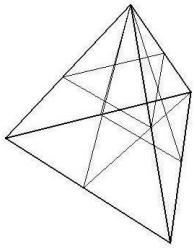

They are used to fill the volume between the surfaces.

Pyramid Elements

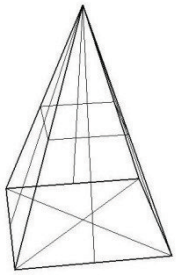

Pyramid elements are used to transition from hexahedral elements to tetrahedral elements.

5.4 Mesh Quality

The quality of mesh is very important for accuracy and stability of computations. The quality criteria that are attributed to meshes in Fluent(Fluent, [7]) are as follows

- Cell squish
- Cell equivolume skew
- Face squish
- Aspect ratio

Cell Squish

It is a measure of deviation in orthogonality with respect to cell faces. It is calculated from the dot product of each vector pointing from the centroid of a cell towards the center of each of its faces, and the corresponding face area vector.

$$\max\left[1-\frac{\overrightarrow{A_i}\cdot\vec{r}_{c0/xfi}}{\left|\overrightarrow{A_i}\right|\left|\vec{r}_{c0/xfi}\right|}\right] \qquad [6.1]$$

$\overrightarrow{A_i}$ is the surface area vector and $\vec{r}_{c0/xfi}$ is the distance between centroid of a cell to its face center. Cell squish of 1 means worst quality cell.

Cell Equivolume skew on Tri/Tetra elements

It is a measure of volume deviation in cells. It is calculated using the formulae

$$\text{Equivolume skew} = \frac{\text{optimal mesh volume-mesh volume}}{\text{optimal mesh volume}}$$

The optimal cell size is the size of an equilateral cell with the same circumradius. Like cell squish a value of 1 means worst quality cell and squish 0 means most desirable cell.

Face Squish

It is calculated from the products of each surface area vector, and the vector that connects the centroids of the two adjacent cells as

$$1 - \frac{\overrightarrow{A_i} \cdot \vec{r}_{c0/c1}}{|\overrightarrow{A_i}||\vec{r}_{c0/c1}|} \qquad [6.2]$$

$\overrightarrow{A_i}$ is the surface area vector and $\vec{r}_{c0/c1}$ is the distance between centroids. Face squish of 1 means worst quality cell.

Aspect Ratio

It is a measure of stretching of a cell. It is computed as the ratio of the maximum value to the minimum value of any of the following distances; the distances between the cell centroid and face centroids, and the distance between the cell centroid and nodes. For a unit cube, the maximum distance is 0.866, and the minimum distance is 0.5, so the aspect ratio is 0.866.

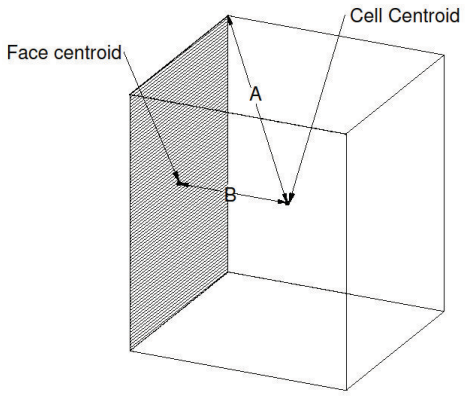

Figure (11) Aspect ratio = A/B

5.5 Turbulence

A mesh which provides accurate results at laminar flow may not be acceptable for turbulent flow situations. It is important to understand the effect of walls in turbulent flows(White, [23]).

5.5.1 Effect of walls on Turbulent Flows

Presence of a wall has significant effects on turbulent flows. In addition to the effect on the mean velocity field because of the non slip conditions at wall, turbulence is changed in other non trivial ways. Very close to the wall viscous damping reduces the tangential velocity fluctuations, while kinematic blocking reduces the normal fluctuations. Toward the outer part of near wall region, the turbulence is rapidly augmented by the production of turbulent kinetic energy due to large gradients in mean velocity.

The profile shape of the near wall region (see figure) as defined by Ludwig Prandtl and Theodre von Karman can be divided as follows:

- Inner layer
- Outer layer
- Overlap layer

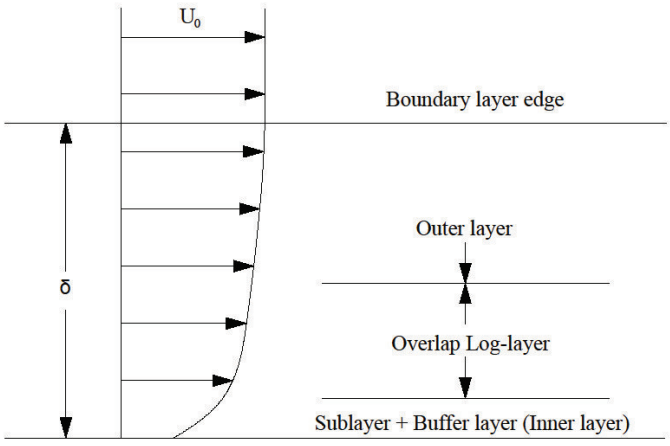

Figure (12) Near wall region profile shape

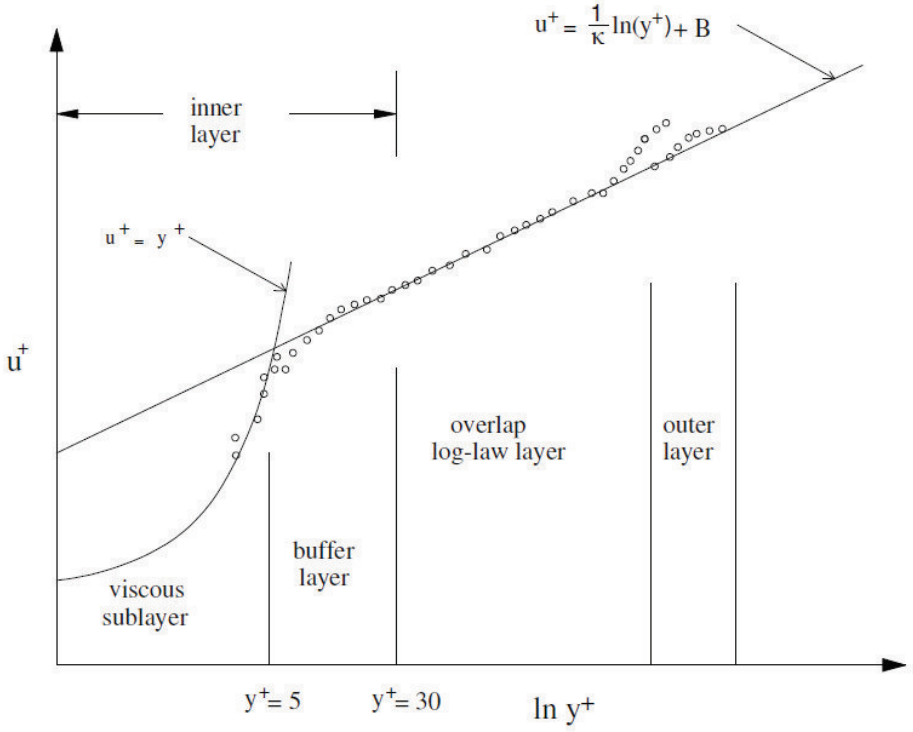

Figure (13) Subdivisions of near wall region

5.5.2 Inner layer

Here viscous (molecular) shear dominates. The flow here is almost laminar. The profile would depend on the wall shear stress τ_w, fluid properties(density ρ, and molecular viscosity μ) and distance y from the wall, but not upon the freestream parameters. Thus, the inner law can be written as

$$\overline{u} = f(\tau_w, \rho, \mu, y) \qquad [6.3]$$

Non-dimensional inner law can be written as

$$\frac{\overline{u}}{v^*} = f\left(\frac{yv^*}{\nu}\right) \qquad [6.4]$$

ν is the kinematic viscosity, v^* is called as the wall friction velocity and is defined as

$$v^* = \sqrt{\frac{\tau_w}{\rho}} \qquad [6.5]$$

5.5.3 Outer layer

In the outer layer turbulent (eddy) shear dominates. The wall acts as a source of retardation of local velocity $\overline{u}(y)$ below the stream velocity U_o. But this reduction of stream velocity is independent of kinematic viscosity μ but dependent on wall shear stress, layer thickness and freestream pressure gradient.

$$U_0 - \overline{u} = g\left(\tau_w, \rho, y, \delta, \frac{dp_o}{dx}\right) \qquad [6.6]$$

Non-dimensional outer law can be written as

$$\frac{U_0 - \overline{u}}{v^*} = g\left(\frac{y}{\delta}, \xi\right) \qquad [6.7]$$

where the local pressure gradient ξ

$$\xi = \frac{\delta}{\tau_w}\frac{dp_o}{dx} \qquad [6.8]$$

and δ is the boundary layer thickness

This is called as velocity defect law. $(U_0 - \overline{u})$ is the defect or retardation of the flow due to wall effect.

5.5.4 Overlap Layer

Both types of shear i.e. molecular and eddy shear are equally important in this layer. The profile connects smoothly with the inner and outer layer.

$$\overline{u}_{\text{inner}} = \overline{u}_{\text{outer}} \qquad [6.9]$$

Non dimensional profile can be written as,

$$\frac{\overline{u}}{v^*} = f\left(\frac{\delta v^*}{\nu}\frac{y}{\delta}\right) = \frac{U_0}{v^*} - g\left(\frac{y}{\delta}\right) \qquad [6.10]$$

The function f contains a multiplicative constant and the function g an additive constant. It can only be true if both f and g are logarithmic functions

Thus for the overlap layer

Inner variables:

$$\frac{\overline{u}}{v^*} = \frac{1}{\kappa}\ln\frac{yv^*}{\nu} + B \qquad [6.11]$$

Outer variables:

$$\frac{U_e - \overline{u}}{v^*} = -\frac{1}{\kappa}\ln\frac{y}{\delta} + A \qquad [6.12]$$

where κ and B are constants for flow past smooth impermeable walls. κ=0.41 and B= 5.0 and A varies with pressure gradient ξ. The terms $u^+ = \frac{\bar{u}}{v^*}$ and $y^+ = \frac{yv^*}{\nu}$ can be defined where u^+ and y^+ are non dimensional velocity and length scales respectively.

5.5.4 Inner Layer Details: The Law of the Wall

Before getting into any detailing of CFD on wall bounded flows it is necessary that one understands the Law of the Wall.

Figure (13) shows how the inner law, rises from no slip at the wall to merge smoothly, at about y^+ to merge smoothly, with the overlap log-law

The inner layer can be further divided into two:

- Viscous Sublayer - At $y^+ \leq 5$, the velocity profile is linear. Here the turbulence is damped out and the boundary layer is dominated by viscous shear.
- Buffer Layer – When $5 \leq y^+ \leq 30$, the velocity profile is neither logarithmic(as in logarithmic overlap layer) nor linear as in viscous sublayer. It is a smooth merge between the two.

Turbulence modeling depends on how well the Inner layer is modeled. To model right up to the inner layer means high computational cost due to increase in mesh size. Hence modeling of the inner layer becomes extremely important, so that a tradeoff between cost and accuracy is achieved.

5.6 Modeling Inner Layer

The k-ε models, the RSM and the LES models are valid for fully turbulent flows i.e flow in the regions far away from the walls. Therefore consideration has to be given to make these models suitable for wall-bounded flows.

Whereas Spalart-Allmaras and k-ω models are suitable to be applied throughout the boundary layer, provided that the mesh is properly resolved.

There are two approaches to modeling near-wall region.

1. Wall function approach
2. Near-wall model approach

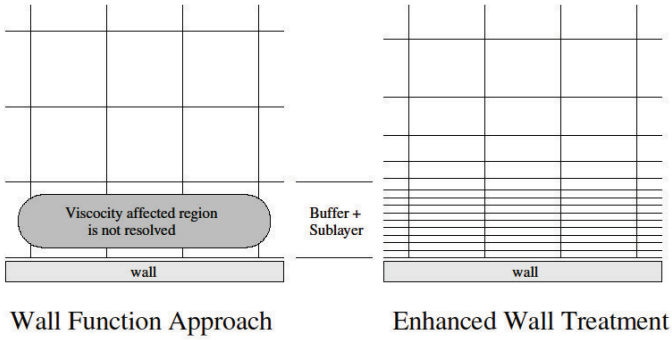

Figure (14) Wall function approach v/s Enhanced wall treatment

Wall function approach

Semi – empirical Wall Functions can be used to bridge the viscosity-affected region between the wall and fully turbulent region(or the log law region). Thus the turbulence models can be used without modifying the mesh for the presence of wall.

For high Reynolds number flows, wall function approach save computational resources and hence is economical. It is also quiet robust.

Near-wall Modeling Approach

The turbulence models can be modified to enable viscosity affected region to be resolved with mesh all the way to the wall. This is called Near Wall Modeling approach.

Wall functions approach cannot be used where low Reynolds number effects are prominent. In such cases wall function approaches ceases to be invalid, necessitating the need for near wall resolution of the mesh. The primary disadvantage of near wall approach is the high computational resource requirement. By resolving the mesh right up to the viscous sublayer, the number of mesh number is increased multifold so that aspect ratios, near the wall region where the gradients are high, can be kept in check.

5.7 Meshed Control Volume

Hexa meshing gives better control, but at the same time it is time consuming and needs a lot more number of meshes than tetra meshes, so that aspect ratio can be kept in check, especially near the blade where the flow gradients are high. Due to limitations in

computational resources tetra mesh was chosen so than standard wall functions and related turbulence model can be used.

Shown below figures or meshed control volume and the blade

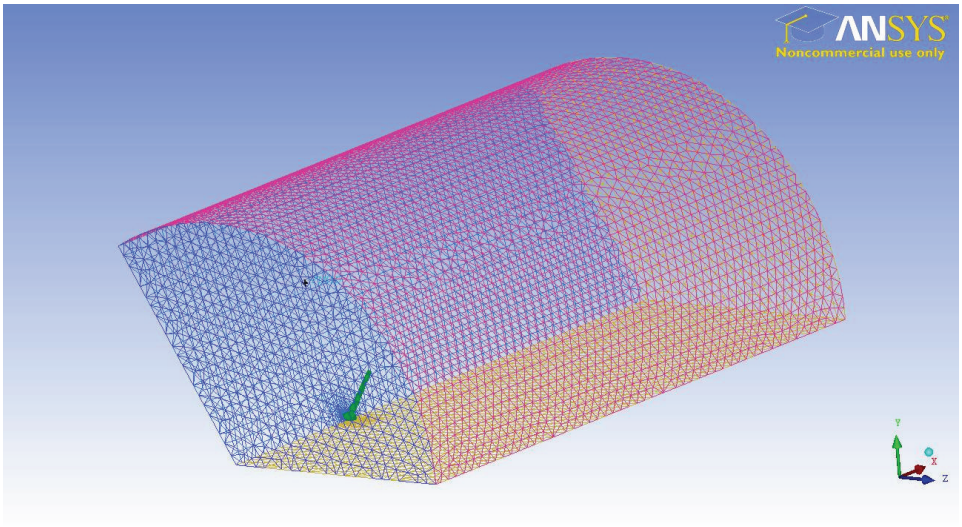

Figure (15) Meshed Domain

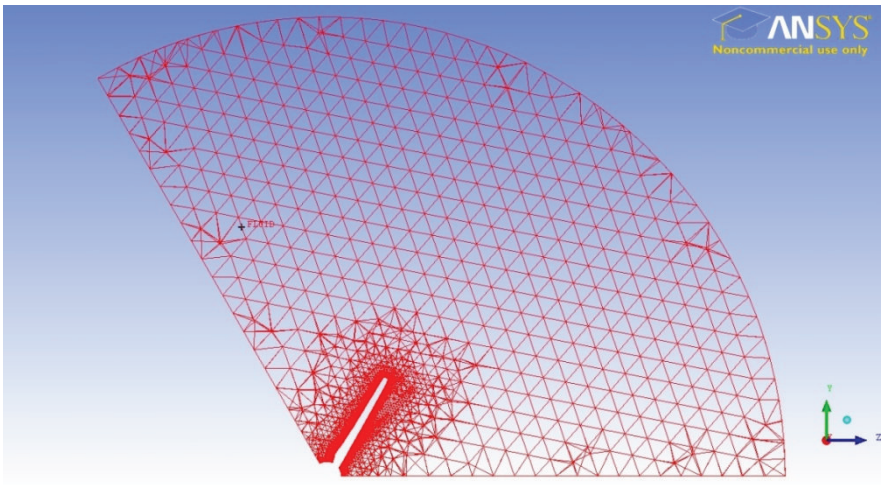

Figure 16 Mesh cut plane at blade section

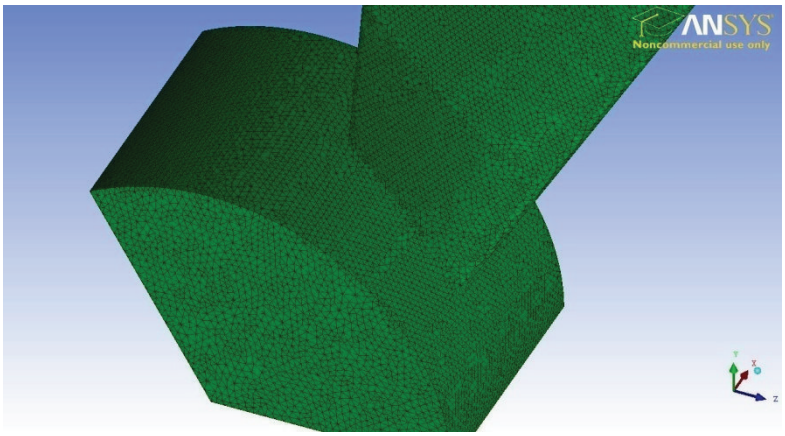

Figure (17) Meshed hub and blade root

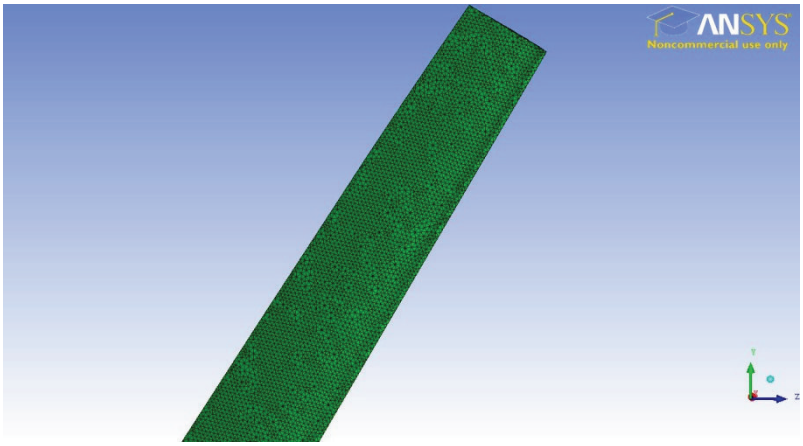

Figure (18) Tetra meshed blade

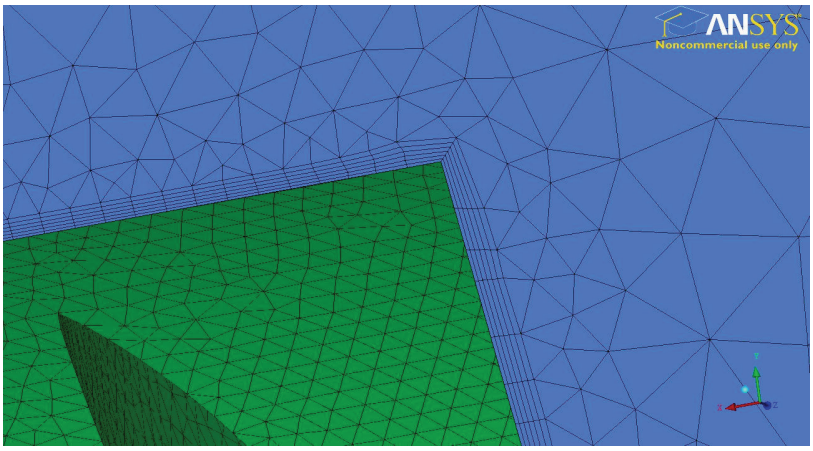

Figure (19) Prism cells for y^+ resolution

6. VALIDATION OF RANS SIMULATION

6.1 Literature Review

With ocean current energy being recognized as an enormous source of energy, related numerical works are experiencing a lot of importance, as the amount of work done on such turbines have been minimal. Hence, any numerical study related to the field will help in validation of experimental data which of late is gaining a lot of steam. This lack in data makes the recent experimental studies by Bahaj and et al (Bahaj, [10][11][12]) on water turbine performance an important benchmark for comparison.

The research by the group focuses on cavitation tunnel and tank tests on a marine current turbine (MCT). Experimental measurements were conducted on a model 800mm diameter turbine in a cavitation tunnel and a towing tank. The experimental data includes measurements of shaft power and thrust of the turbine for a series of blade pitch settings and speeds. The best C_P values in the test was noted at pitch angle of 20 degrees as it gave a very smooth curve for various TSRs .

A scaled up version of the blade with 3000mm diameter (see chapter 4 for the blade characteristics) is used for the analysis and the results are validated with experimental result for the best case.

6.2 Mathematical model

The mathematical model includes the continuity and momentum equations. These equations are solved using a single moving reference frame attached to the rotor blades, with the assumption of incompressible and turbulent-steady flow. Basically, they are the incompressible steady-RANS classical equations. The k-ε model with standard wall functions was used in all simulations.

As the code solves the incompressible flow equations, no equation of state exist for the pressure, and the Coupled algorithm was adopted to enforce the pressure-velocity coupling. Second order discretization scheme was chosen for continuity and momentum equations.

6.3 Computational Mesh and Domain

All the blade peripherals like shaft and mooring structure was not modeled for simplicity. Periodicity property was used to mesh volume for the three bladed rotor. 120 degrees periodicity of the rotor was exploited, by only meshing the volume around one blade. Periodic boundaries as explained in chapter 3 was applied for including the other two blades.

The pre-processor ANSYS ICEM CFD was used to build a tetrahedral mesh of approximately 0.85 million volumes. As far as possible y^+ values were adjusted to be within 30 to 300 so that standard wall functions can be used. By doing this a reasonable compromise between computational cost, time and accuracy is established.

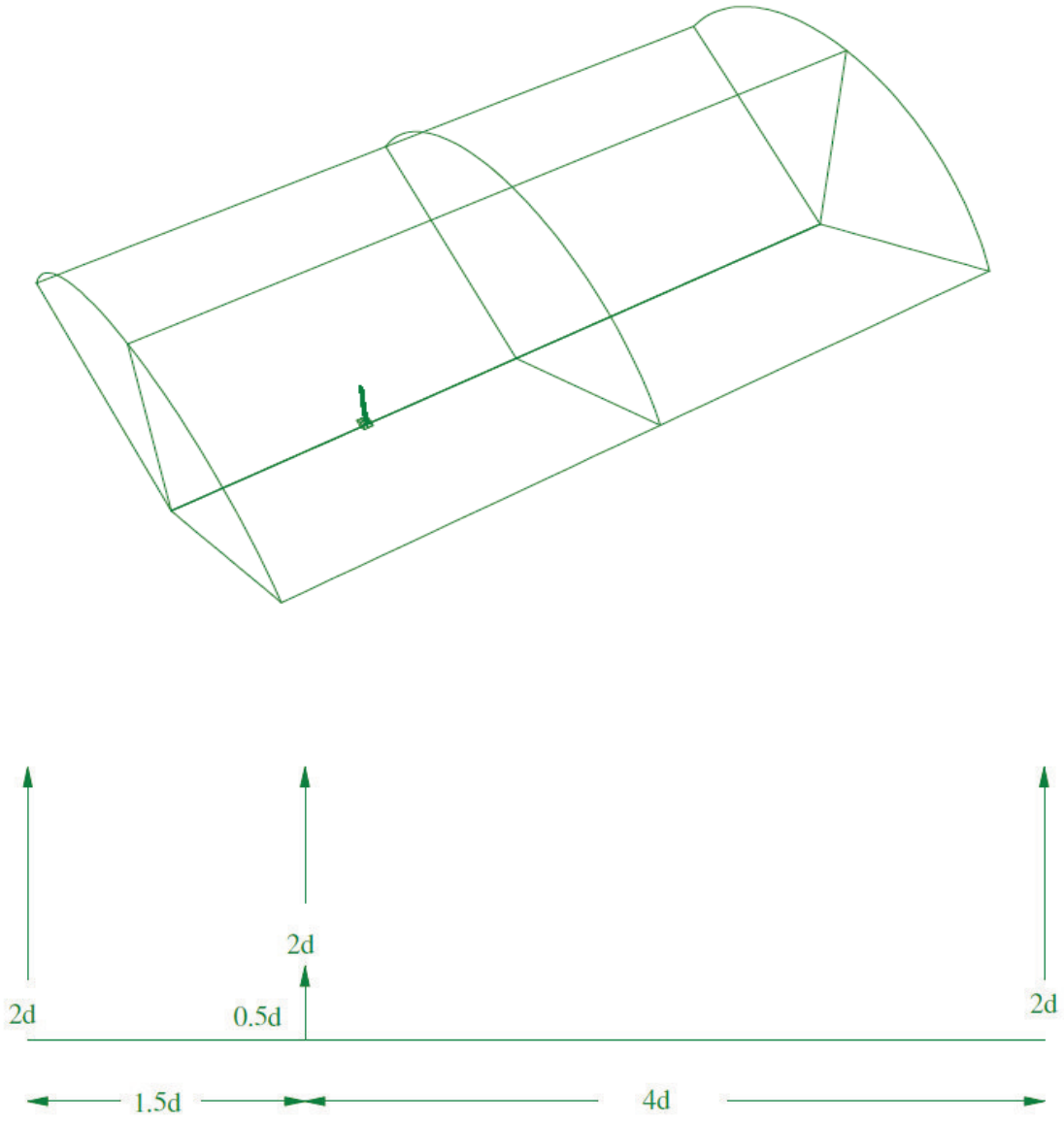

Figure (20) Computational domain

The computational domain was taken as cylindrical with a diameter of 4d, where d is the rotor diameter. Inflow boundary was applied for inlet at distance of 1.5d from the turbine and a uniform velocity was applied. Outflow boundary was applied at the outlet spaced at

a distance of 4d from the turbine. The boundaries were placed at locations as shown in the figure (20).

6.4 CFD v/s Experiment

The commercial code Fluent was used in all the calculations. To validate the numerical model, the overall performance for the turbine was computed and compared to the experimental results (Bahaj, [11]).

It is always convenient to express the performance by means of non-dimensional, characteristic performance (power coefficient) as a function of tip speed ratio. The coefficient of power was calculated and plotted against varying TSR. The TSR is varied by increasing the rotational velocity by maintaining the inflow velocity of the rotor.

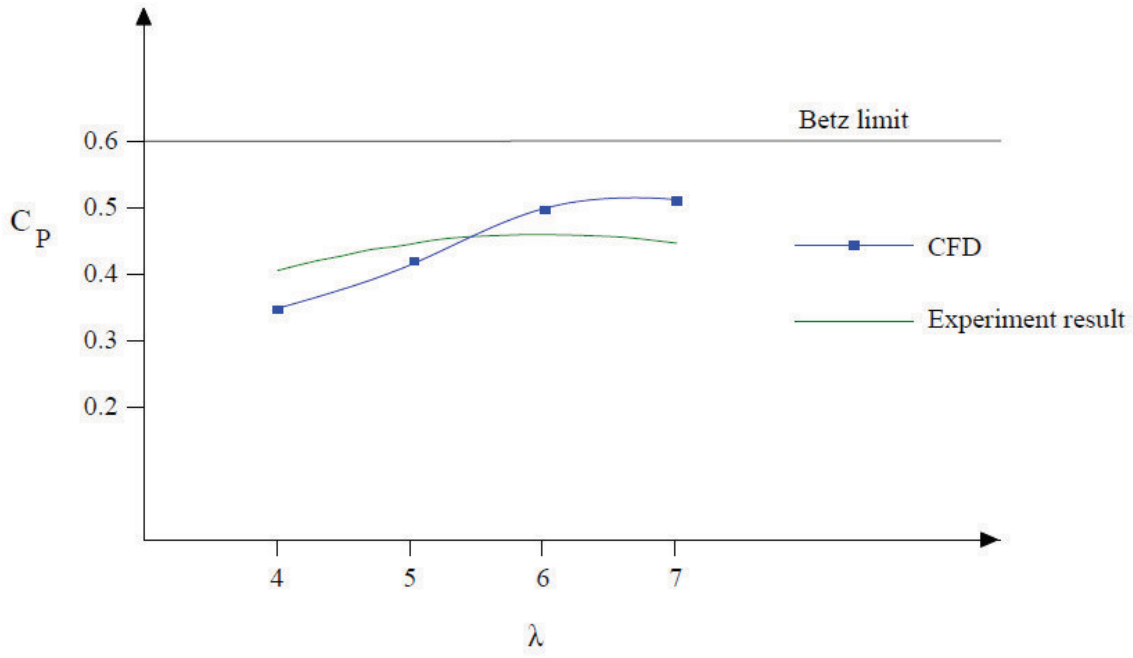

Figure (21) C_p v/s λ for experimental and CFD results

Still the results show that the C_P curve bears a similar trend in both CFD and experimental study. The maximum computed C_P is about 0.512 achieved at TSR 7. The value is much less than the Betz limit, due mainly to drag and tip losses for the flow conditions. For higher TSR's there are discrepancies and unsteady simulations will have to be done.

Figure (21) above shows the calculated C_P in CFD in comparison with the experimental studies. As mentioned before, only one case was taken into consideration for validation. An error of 11% in the maximum C_P is observed.

For greater accuracy turbulence models such as k-ε model can be used. It has been made suitable to the present case with the help of standard wall boundary conditions. In actual k-ω SST should be used so that the boundary layer effects are properly captured. Because k-ω SST requires enhanced wall treatment it makes it computationally expensive and time consuming. And given the resources, only standard wall functions could be used.

7. FLOW FIELD AND EDDY VISCOSITY

This chapter deals with the affect of flow on the blade, its surrounding area and the wake of the turbine. A comparison on the axial velocity distribution for different pitch angles for a given TSR with a fixed inflow velocity is presented. Also a comparison is presented for velocity distribution for varying TSR with fixed in pitch angle.

7.1 Flow Field

The effect of turbine on the flow is being studied. Of importance will be the flow effect behind the turbine i.e. the wake of the turbine.

A case with TSR 5 and a pitch angle 20 □ is taken for studying the flow characteristics. The stream velocity is fixed at 1.73 m/s and the blade has a rotation of 2.883 rad/s. The flow is modeled with a moving reference frame with the flow rotating around the blade. The turbine (wall boundary condition) is modeled as moving wall with a velocity of zero. By doing this an unsteady case has been made into a steady state.

The axial, tangential, and radial velocity contours are plotted in different sections along the x axis. Also plotted along with it is velocity contour plot along the axial direction. A plot for velocity profile radially starting from hub centre to domain extent is also presented.

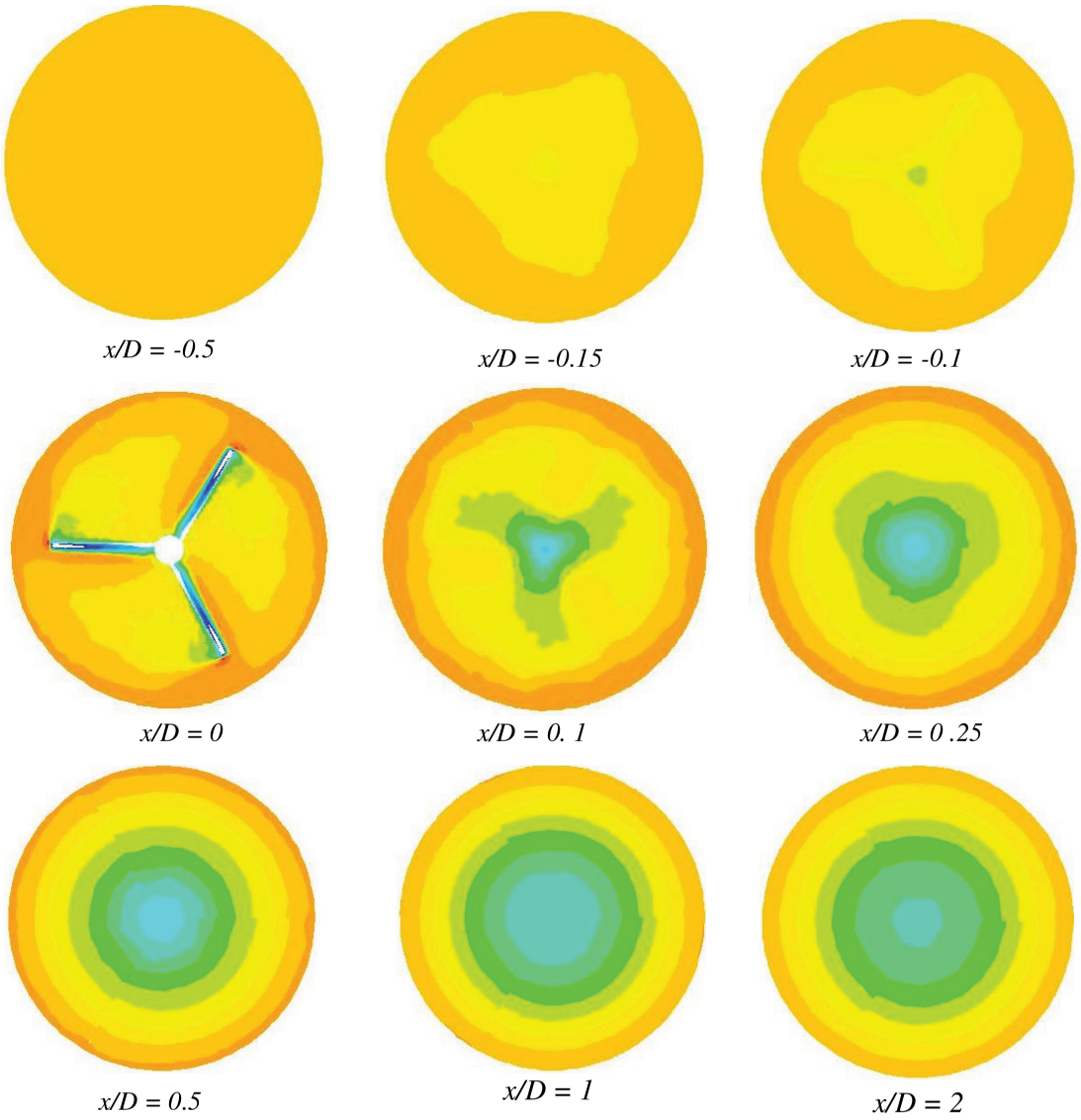

Figure (22) Axial velocity contours at various axial (x) locations for TSR 5 with axial velocity = 1.73 /sec

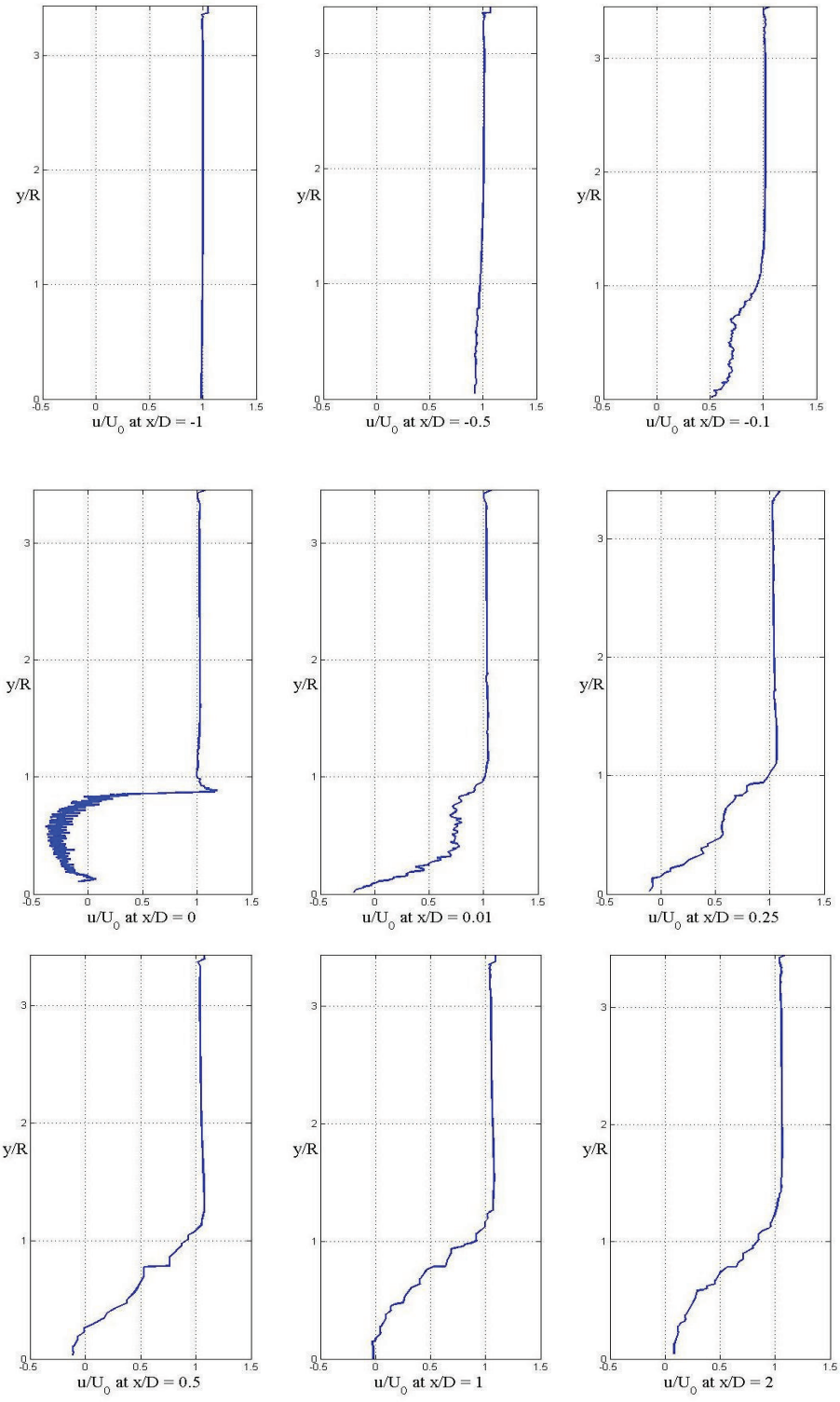

Figure (23) Axial velocity plot along radial lines from hub center to domain extends at various x/D locations U=1.73 m/s TSR=5

'x' is the horizontal axis i.e. the axis parallel to the flow and 'y' and 'z' are the axes perpendicular to the flow. R and D are the radius and the diameter of the rotor respectively. Figure (22) shows axial velocity contours at different x locations. The contours are plotted from rotor center to a radially outward distance of 4m so that only the near blade region can be visualized. The axial velocity reduces as the flow approaches the rotor. This is because of the back flow occurring from the turbine surface (modeled as wall). At the plane x=0, in the presence of the rotor the axial velocity is reduced in the rotor swept area. This is an indication of the axial induction factor as shown in the actuator disk theory. Downstream of the propeller there is an area of zero or sub zero velocity. This is mainly due to the presence of the hub which is blunt (as it was modeled for simplicity), because of which there is a void created and the flow might get disturbed in that area. The expansion of wake is not visible clearly in this figure.

Figure (23) shows the axial velocity plots at various axial locations taken at radial lines inclined at an angle of 60 degrees to the 'z' axis. Again, the reduction in velocity before the turbine is an interesting observation. The reduction is more near the hub area. The bluntness of the hub accounts for this. Here the expansion of the wake behind the turbine can be visualized. Downstream of the turbine, the location at which the velocity reaches the far stream velocity U_0 shifts further outward radially as the flow advances. Behind the turbine, there is an area of negative velocity, largely due to the mixing of the flow stream as explained earlier.

The expansion of the wake can be seen in the figure (24) below. The figure shows the axial velocity contour on x=0 plane, which cuts through the turbine i.e. inclined at angle of 60 degrees to the turbine.

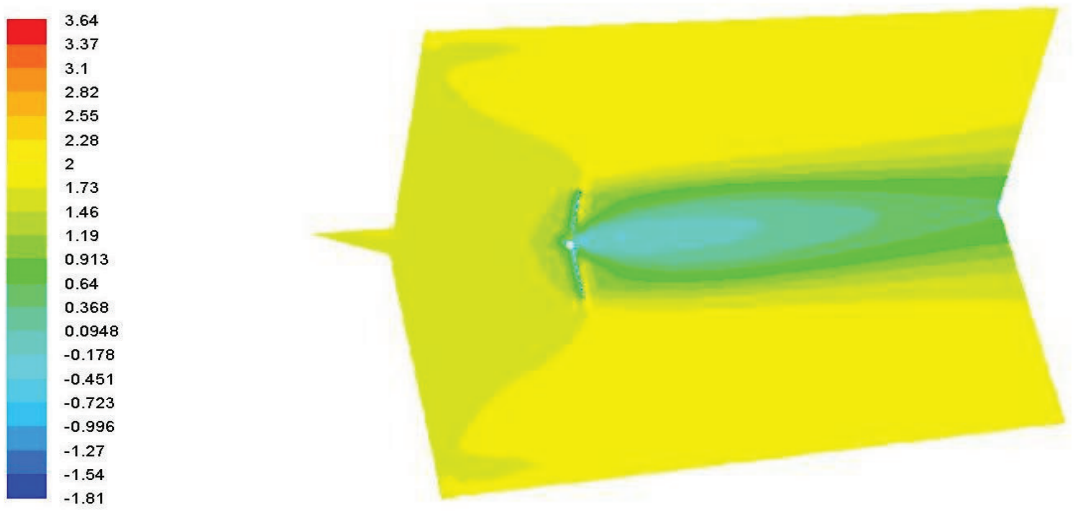

Figure (24) Axial velocity(m/s) contour showing wake expansion on a plane aligned with the blade

Clearly, from the above figure, the wake expands as the flow moves downstream. The outflow boundary as explained earlier is at a distance of 4D. Even at the outflow, there are regions with extremely low velocities. It implies that if a turbine is to be kept in the wake it has to be for sure, at a distance greater than 4D. More experiments have to be done to find out the exact distance to keep the next rotor.

Figure (25) shows the reduction of axial velocity along the flow direction for different TSRs, which is in conformance with actuator disk theory and is an excellent check. Space averaged values of the velocity are plotted against axial direction.

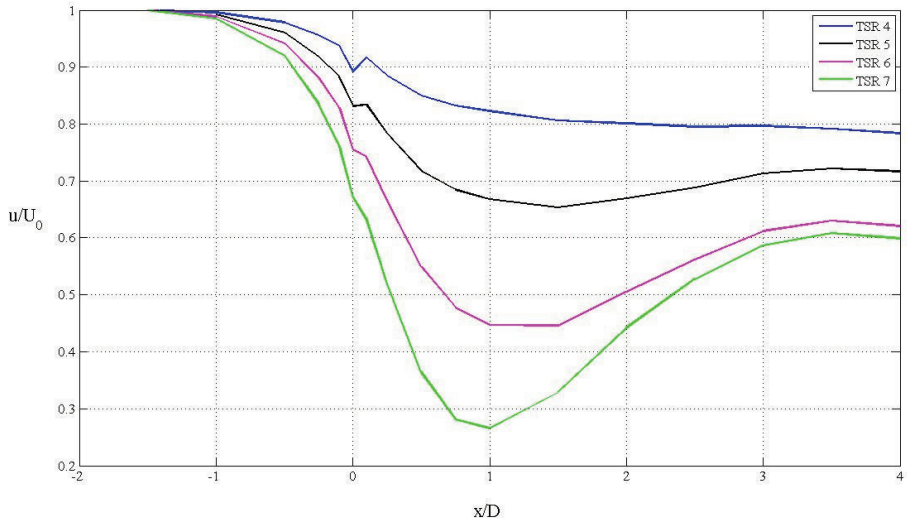

Figure (25) Non dimensionalised axial velocity plot along x direction

Given below is Figure (26) of path lines of particles released from the turbine surface, colored by the velocity magnitude. The front and the isometric views are shown. The particles initially move outwards and then start to constrict. Near the hub they are a lot of disturbances owing to the bluntness of the modeled hub.

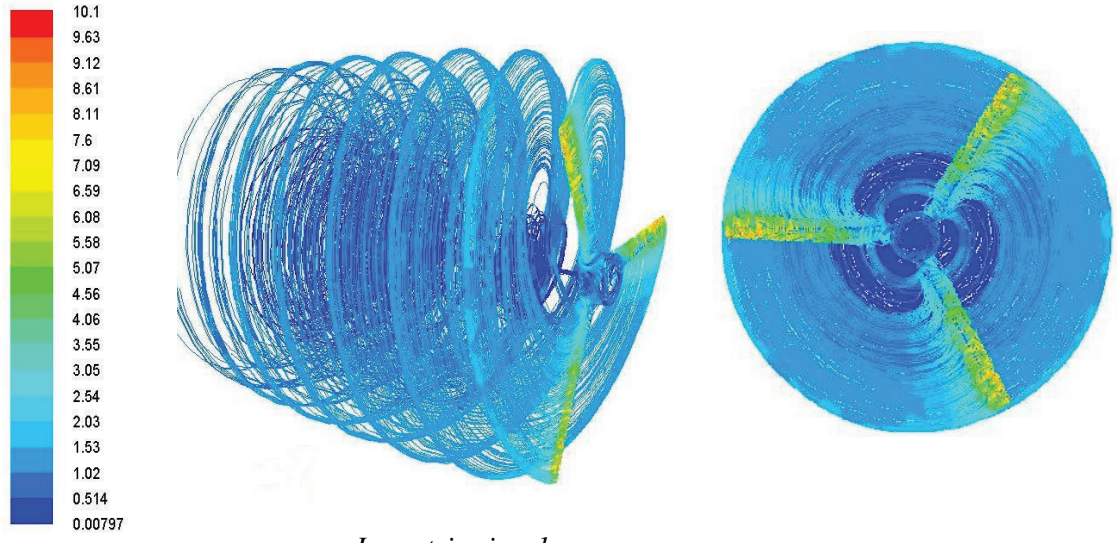

Figure (26) Pathlines of particles from the turbine colored by velocity magnitude

In addition to study of axial velocities, radial and tangential velocities are done.

Figure (27) shows contour plots of radial velocities at various axial locations. Ideally an increase in radial velocity will be observed in area where the axial flow is obstructed by a boundary. This increase accounts for satisfying continuity. As expected maximum variation of radial velocity is observed near the blade. Near the blade tip there is considerable increase in the radial velocity. This is because of the cross flow effect over the top of the tip. At about 0.25D effect of radial velocity subsides and the flow field is no longer affected by the radial movement of particles. Similarly the disturbance before the turbine starts at about x= -0.15D. Another interesting observation is that beyond 4m radius from the hub center, there is no inward movement of the flow. In effect, radially the flow field is affected in a region bounded by r = 0.67D and not more.

Figure (28) shows contours of tangential velocity vectors. Like radial velocity, effect of variation in tangential velocity is limited to a small region axially. The disturbances are observed from x=-0.1D to x=0.2D. Tangential velocity as expected increases along the blade. Figure (29) shows the variation of tangential velocity along the blade radius. There is no velocity at the hub and it increases to a value of 8.3 m/sec, which is equal to the relation ωR. The velocity plotted are negative in magnitude, which is a direct reflection of the input rotational velocity for making the turbine rotate in clockwise direction. The tangential velocity effects are prevalent no more than the blade radius area.

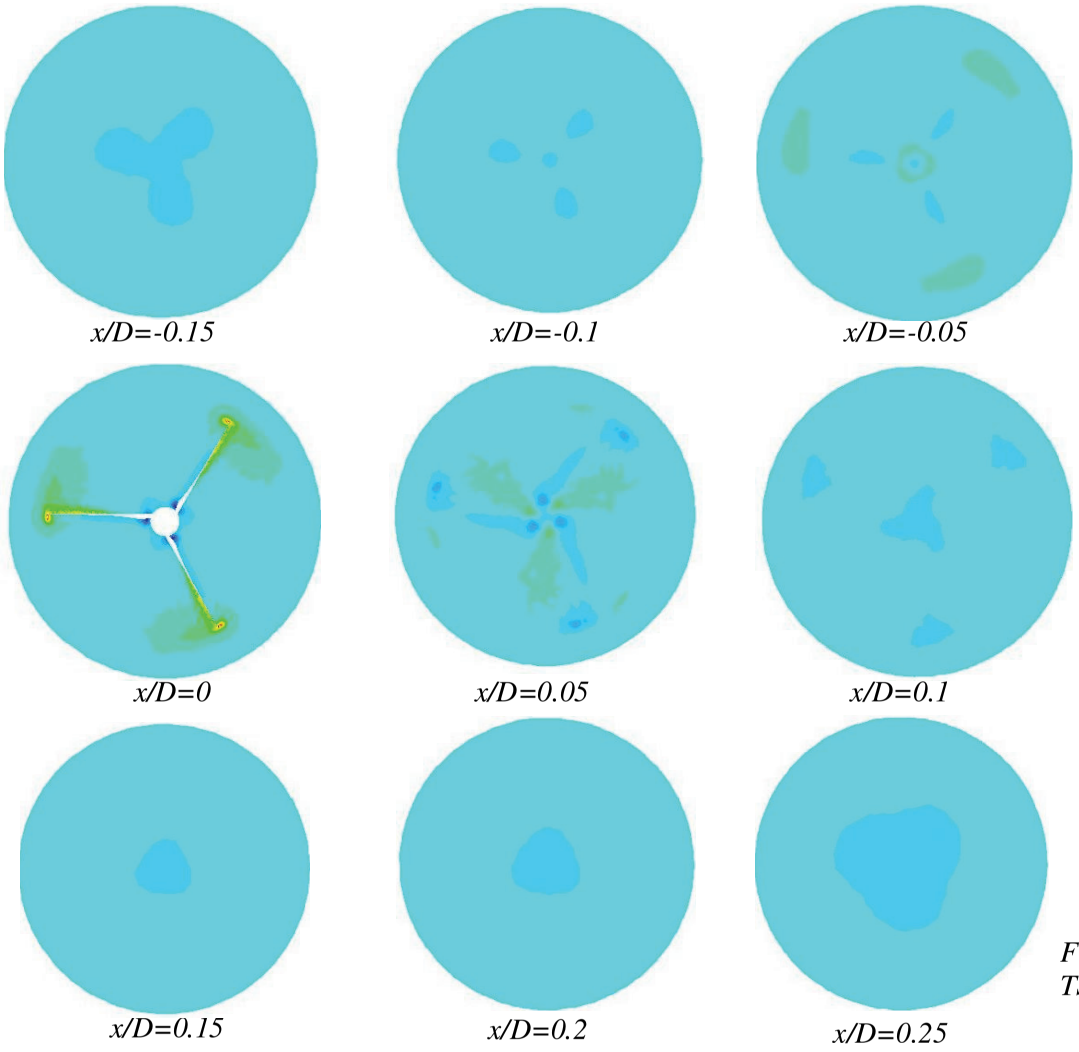

Figure (27) Radial velocity contours at TSR=5 and U_o =1.73 m/s

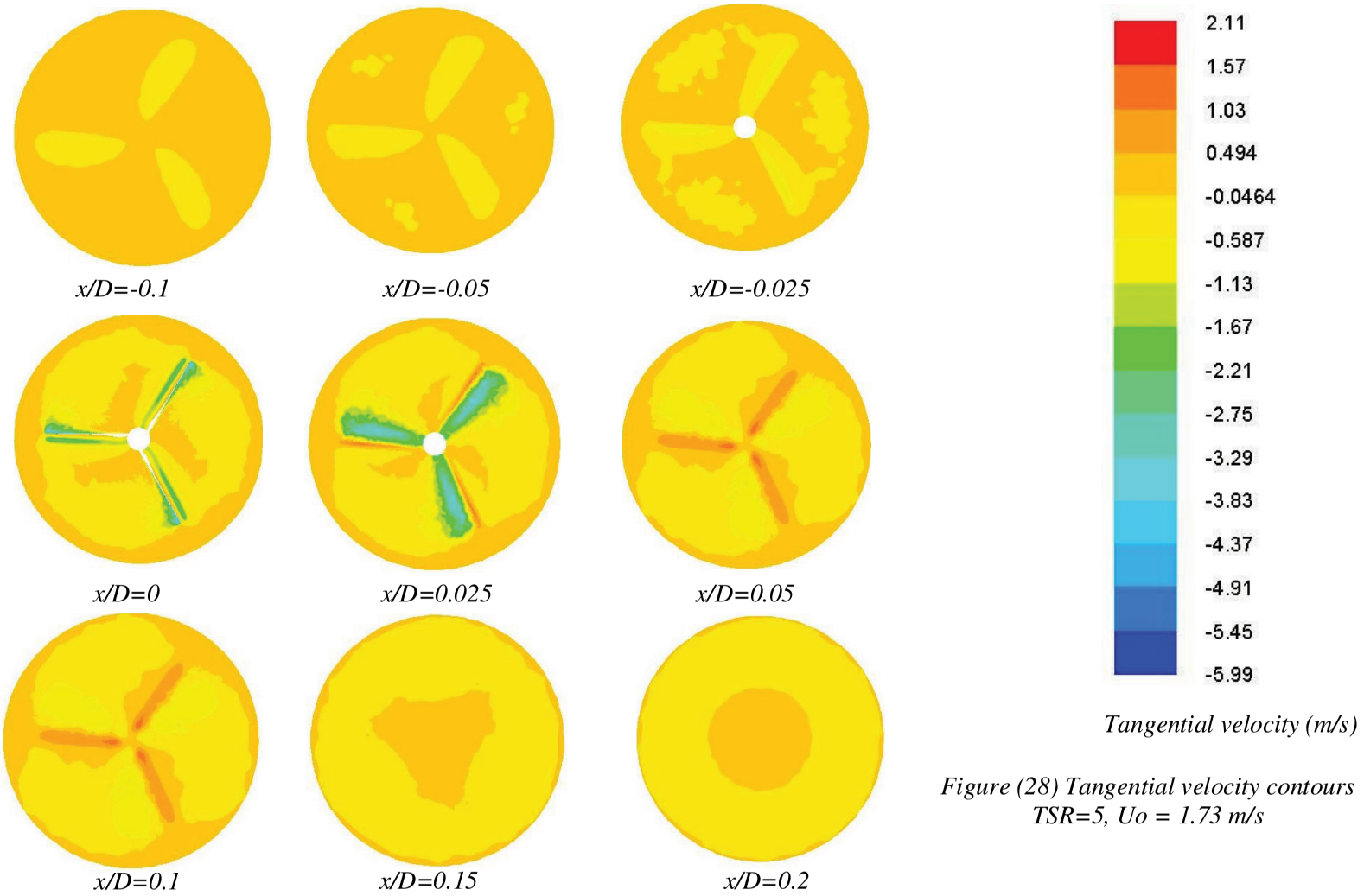

Figure (28) Tangential velocity contours
TSR=5, Uo = 1.73 m/s

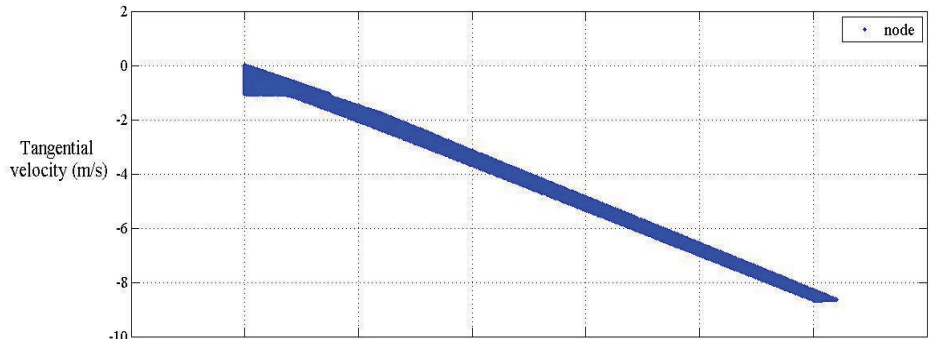

Figure (29) Tangential velocity along the nodes on the turbine

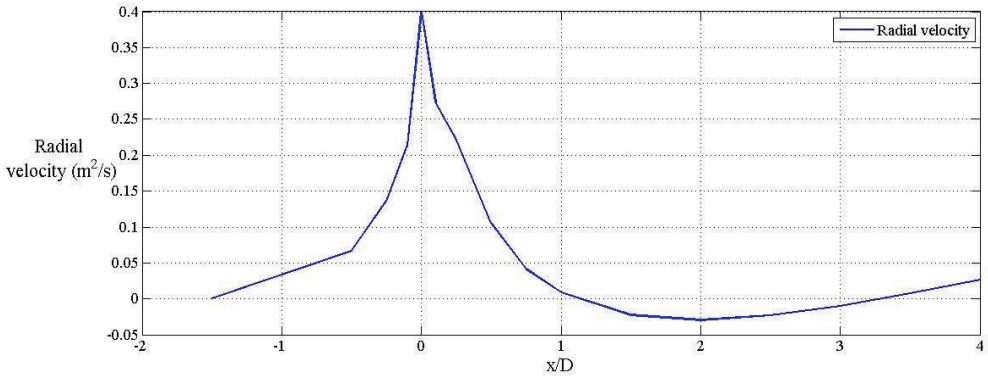

Figure (30) Radial velocity along the axial direction

Figure (30) shows the variation of radial velocity along flow direction. As expected, to compensate the decrease in axial velocity the plot shows a sharp rise in value near the turbine.

7.2 Comparison of Flow for Pitch and Velocity Profiles Variations

Since it is the axial velocity profile which decides the amount of energy extracted by a turbine, a comparison of the profiles for different pitch angles and velocity profiles should give a good estimate about the flow characteristics in varied environments.

Two sets of comparisons are done.

1. The pitch angle is varied from as 15, 20 and 25 degrees with uniform inflow velocity.
2. The velocity profile is given a shear and then compared with the results of uniform velocity profile.

7.2.1 Varied Pitch Angle

The angle at the hub-blade intersection is assumed to be the pitch angle of the turbine. Three different angles are taken for the analysis – 15, 20 and 25 degrees. The simulation is done at a uniform inflow velocity U_0 = 1.73 m/s and all the cases are run at a TSR of 5 i.e with a rotational velocity 0.2883 rad/s. The plots shown here are taken at same locations in all the simulations with similar operating conditions. These are axial velocity plots at radially outward lines along the blade direction. The velocity and grid directions are non dimensionalised for comparison purpose.

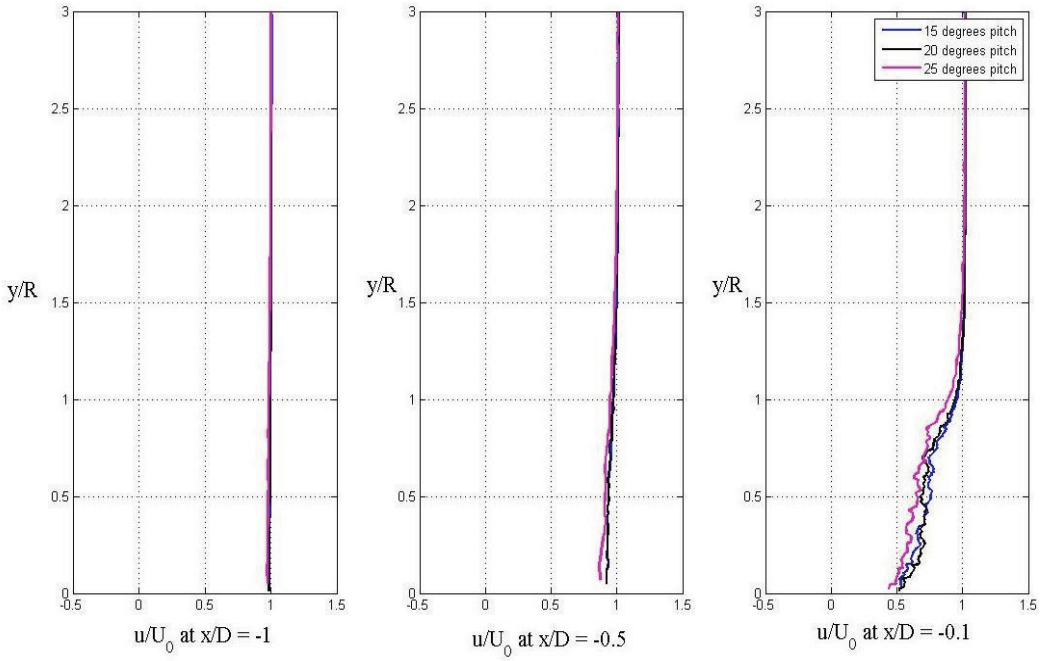

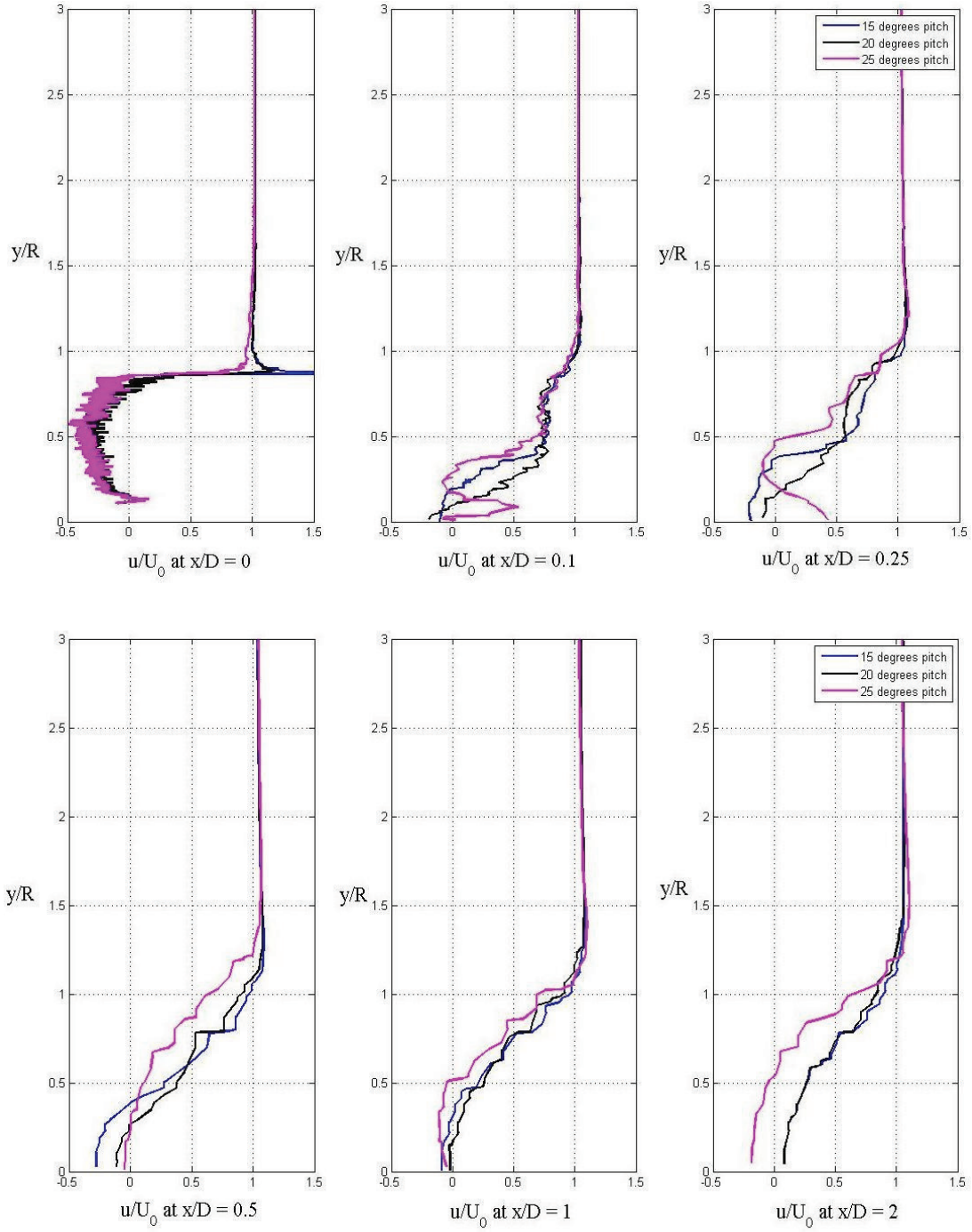

Figure (31) Axial velocity plot along radial lines from hub center to domain extends at various x/D locations for different pitch angles U=1.73 m/s TSR=5

The plots show similar trend in the velocity profiles for pitch angle of 15 and 20 degrees. But for 25 degrees there is a lot of disturbance after the turbine. All the curves point to expansion of wake and hence positive power extraction.

7.2.2 Sheared Velocity Profile

A comparison is done with a velocity profile as shown in the figure (32). A linearly varying profile is considered. Axial velocity plots as before are compared with uniform flow velocity plots. A velocity of zero is considered at a distance of 2D below the turbine and it grows linearly towards and reaches a velocity U_0, free stream velocity as considered in the other case. The case is run at a TSR of 5 for a turbine with a pitch angle of 20 degrees.

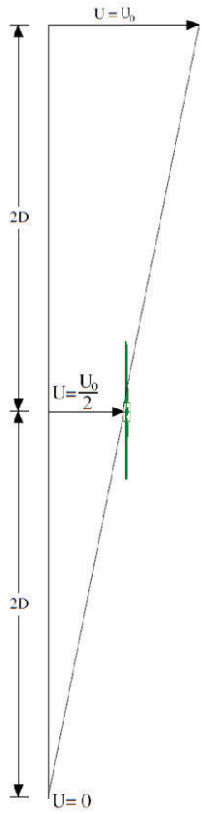

2) Profile

The plots are shown along a line which propagates radially outwards from the hub center to the domain extend. These lines are place at an azimuthal direction parallel to the blade alignment.

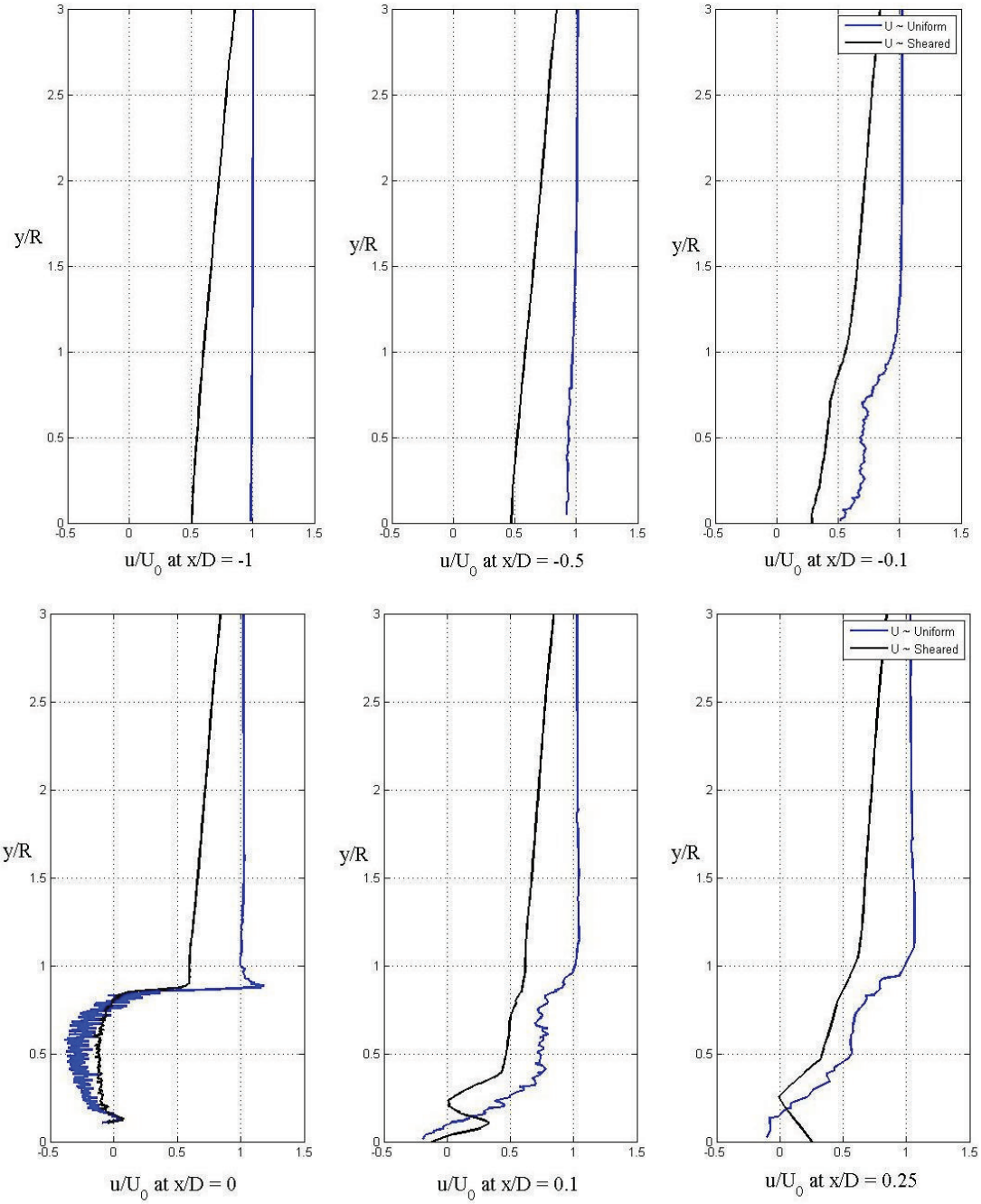

Figure (33) Axial velocity profile comparing uniform and sheared flow. TSR=5, U_0=1.73 m/s

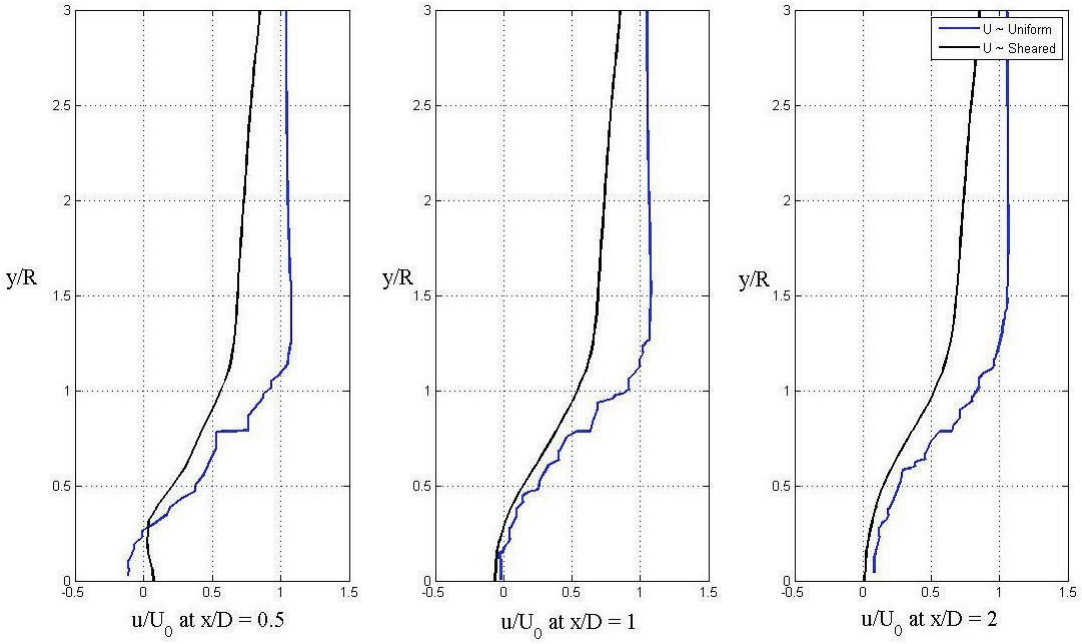

Figure (34) contd. Axial velocity profile comparing uniform and sheared flow. TSR=5, U_0=1.73 m/s

Interestingly in both the cases the profile looks more or less stable after x/D = 0.5 and is advancing to the initial far field state. In the case of sheared flow, there are disturbances at x/D = 0.5. The velocity for sheared flow condition seems to be reaching the fully developed condition faster than the one with uniform flow. This is because the average flow velocity in the sheared flow is almost half that of the flow velocity in uniform flow, hence there is lesser power extraction from the flow.

7.3 Eddy Viscosity

The turbulent transfer of momentum by eddies give rise to an internal fluid friction, in a manner analogous to the action of molecular viscosity on laminar flows. Eddy viscosity is a function of the flow, not of the fluid. It is greater for flows with more turbulence. The value of eddy viscosity can reach upto 10^{-2} m/s^2.

Two cases are taken for visualizing the formation of eddies and it effects - A pitch angle of 15 degrees with a uniform flow velocity of 1.73 m/s and a sheared flow as shown in figure (34) for a pitch angle of 20 degree. TSR 5 has been chosen for the case.

Given below is the contour plot of the turbulent viscosity along a plane cutting thru the turbine as seen from inlet to outlet direction

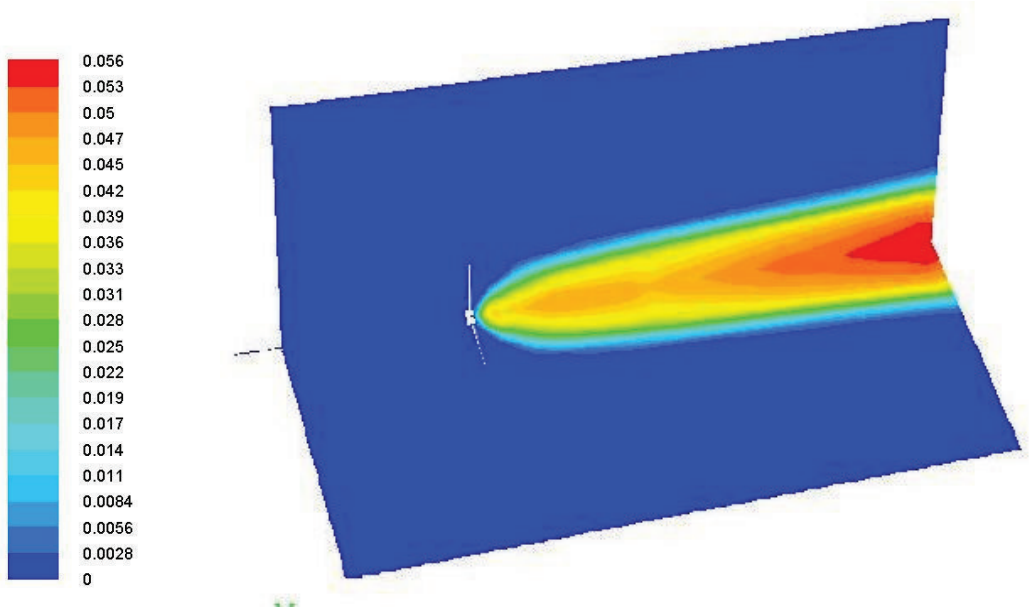

Figure (35) Contours of turbulent viscosity from inlet to outlet along a section parallel to the flow and cutting thru the blade TSR=5, U_0 = 1.73 m/s

υ_T develops across the blade and increases in magnitude along the wake of the turbine. Further downstream will have to be analysed to know exactly how far in the wake does the effect remain.

A comparison between the two cases as described earlier is given in the following figure. Average turbulent viscosity values are plotted along the axial direction in figure (33).

The average flow velocity in the sheared flow is half that of the uniform flow velocity. The dip in eddy viscosity formation is the reflection of this difference in viscosity value.

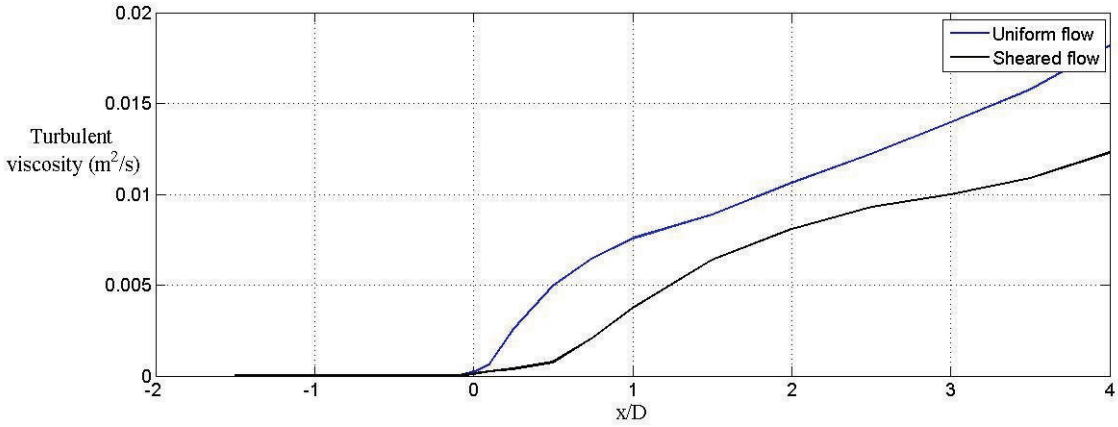

Figure (36) Turbulent viscosity for sheared and uniform velocity profiles

More cases can be analyzed in a similar manner as a future work, which should give a good approximation of the amount of viscosity created and perhaps a model formulated.

8. CONCLUSION

In this research work, a generic study of a RANS model of flow past an ocean current turbine has been investigated. The model has been validated against the results of an experimental study by Bahaj et al (Bahaj,[10]). Considerable accuracy was found on comparison of the power coefficient, with a maximum power coefficient at about tip speed ratio 7.

A study of the flow field has been carried out. The variations of the velocity components, radial, axial and tangential, have been investigated. Wake expansion has been determined. The reduction in axial flow velocity as the fluid moves past the turbine is in consistence with theory. It was found out that tangential velocity effects decays faster than the radial velocity effects. Radial velocity is seen to peak at blade location. A comparison of the velocity profiles for different hub pitch angles at different sections of the control volume was performed. A study of the flow with a shearing velocity profile was carried out and a comparison with uniform flow was conducted.

Eddy viscosity calculation and its comparison with two different kinds of flows – a uniform flow and a sheared flow were conducted. Eddy viscosity being a function of flow velocity is found to have higher magnitude in uniform flow field than the shearing flow field which had a mean velocity less than the former case.

As future work, use of higher performance computers can be used for RANS simulations of greater accuracy. Various flow field conditions involving variation of parameters like flow velocity, flow profiles, density stratification, etc, together with turbine characteristics can be studied. The effect on eddy viscosity in such conditions can be studied and mathematical models can be generated to account for eddy viscosity distribution. With proper mesh resolution very high degree of accuracy can be achieved.

BIBLIOGRAPHY

[1] Stommel H.M., *The Gulf Stream: a physical and dynamic description,* Edition 2, University of California Press, 1976.

[2] Knauss, J. A., *Introduction to Physical Oceanography*, Edition 2, Prentice-Hall, Inc., 1997

[3] Hanson et al., Hanson, H.P., Skemp, S.K., Alsenas, G.M., and Coley, C.E.*, 2010: Power from the Florida Current: A New Perspective on an Old Vision.* Bulletin of the American Meteorological Society 87(7), in press.

[4] NASA, "NASA Science- Earth", Ocean Currents http://science.nasa.gov/earth-science/oceanography/physical-ocean/currents/

[5] COET, "Center for Ocean Energy Technology" http://coet.fau.edu/

[6] COET, Driscoll, F. R., Skemp, S.H., Alsenas, G.M., Coley, C.J., Leland, A., *Florida's Center for Ocean Energu Technology*

[7] OCS, "OCS Alternative Energy and Alternate Use Programmatic EIS" http://ocsenergy.anl.gov/guide/current/index.cfm

[8] Kuik, G.A.M., *The Lanchester-Betz-Joukowsky Limit*, Wind Energy 10, 2007, 10pp. 289-291

[9] Xiros, M.I and Xiros N.I, *Remarks on Wind Turbine Power Absorption Increase by Including the Axial Force due to the Radial Pressure Gradient in the General Momentum Theory*, Wind Energy, Wiley Interscience, 2007

[10] Bahaj, Batten, W.M.J., Bahaj, A.S., Molland, A.F., Chaplin, J.R., *Hydrodynamics of marine current turbines*, Renewable Energy 31, Elsevier Ltd., 2006, pp. 249-256

[11] Bahaj, A.S., Batten, W.M.J., Molland, A.F., Chaplin, J.R., *Power and thrust measurement of marine current turbines under various hydrodynamic flow conditions in a cavitational tunnel and towing tank*, Renewable Energy 32, Elsevier Ltd., 2007, pp. 407-426

[12] Bahaj, Batten, W.M.J., Bahaj, A.S., Molland, A.F., Chaplin, J.R.*The prediction of the hydrodynamic performance of marine current turbines*, Renewable energy 33, Elsevier Ltd., 2008, 1085-1096

[13] Camporeale, S.M. and Magi, V., *Stream Tube Model for Analysis of vertical Axis Variable Pitch Turbine for Marine Energy Conversion*, Energy Convers. Manage.,2000, pp. 1811-1827

[14] Calcagno, G., Salvatore, F., Greco, L., Moroso, A., and Erickson, H., *Experimental and Numerical Investigation of an Innovative Technology for Marine Current Exploitation: The Kobloid Turbine*, Proceedings of the International Offshore and Polar Engineering Conference, pp. 323-330.

[15] Ponta, F.L and Jacovkis, P.M., 2001, *A vortex Model for Darrieus Turbine Usinf Finite Element Techniques*, Renewable Energy 24, pp 1-18

[16] Goly, A., *Hydrodynamic analysis of ocean current turbines using vortex lattice method*, FAU, 2010

[17] Li, Y., Calisal, M.S., *A discrete Vortex Method for Simulating a Stand Alone Tidal Current Turbine: Modelling and Validation*, Journal of Offshore Mechanics and Artic Engineering, 2010

[18] Anderson, J.D.Jr., *Computational Fluid Dynamics – The basics wit h Applications*, McGraw-Hill, 1995

[19] Fluent, *ANSYS FLUENT 12.0 Theory Guide*, ANSYS Inc., April 2009

[20] Launder, B.E. and Spalding, D.B., *Lectures in Mathematical Models of turbulence*, Academic Press, London, England, 1972

[21] Maxwell, J.F., McGowan, J.G., and Rogers A.I., *Wind Energy Explained*, John Wiley and Sons Ltd, Chichester, London, England, 2007

[22] Chmltech, “CFD Grid Generation Methods”, http://www.chmltech.com/cfd/grid_generation.pdf

[23] White, F.M., *Viscous Fluid Flow*, Edition 2, McGraw-Hill, Inc., 1991